TECTONICS, VOL. 31, TC1008, doi:10.1029/2011TC002981, 2012

Timing of extension in the Pioneer metamorphic core complex with implications for the spatial-temporal pattern of Cenozoic extension and exhumation in the northern U.S. Cordillera

James J. Vogl,[1] David A. Foster,[1] C. Mark Fanning,[2] K. Allen Kent,[1] David W. Rodgers,[3] and Timothy Diedesch[4,5]

Received 5 July 2011; revised 21 November 2011; accepted 29 November 2011; published 9 February 2012.

[1] The Pioneer core complex (PCC) in central Idaho lies along a transition between Early Eocene and ca. ≤40 Ma core complexes to the north and south, respectively. Thus, the age of extensional development of the PCC is important in understanding the spatial-temporal patterns of core-complex development in the North American Cordillera. New results, including structural observations and U-Pb zircon (SHRIMP and ICPMS) geochronology, constrain the early extensional history of the footwall for the first time. High-temperature strain with a top-WNW shear-sense is pervasive throughout metamorphic rocks of the northwestern footwall. An isoclinally folded dike yields a crystallization age of ~48–47 Ma, whereas a crosscutting dike yielded an age of 46 Ma. Metamorphic rocks are also intruded by the ~50–48 Ma Pioneer intrusive suite (PIS), a W-dipping granodiorite sheet displaying a magmatic fabric. Northwest-trending lineations are locally visible and also defined by anisotropy of magnetic susceptibility, indicating that during emplacement, the PIS was undergoing similarly oriented extensional strain as the enclosing metamorphic rocks. Therefore, WNW-directed extension spanning this structural section occurred between ~50 and 46 Ma. Following emplacement of crosscutting 46 Ma dikes, deformation was partitioned into the WNW-directed Wildhorse detachment. Motion on the detachment occurred between ~38 and 33 Ma, as documented by previous $^{40}Ar/^{39}Ar$ thermochronology. It is not clear, however, whether extension was continuous through the interval between these two time periods. Although Early Eocene extension in the PCC was synchronous with extension in core complexes to the north, rates of footwall exhumation in central Idaho were much lower. This southward slowing is compatible with N-S differences in inferred subduction zone geometry/kinematics and in the internal character of the orogenic wedge.

Citation: Vogl, J. J., D. A. Foster, C. M. Fanning, K. A. Kent, D. W. Rodgers, and T. Diedesch (2012), Timing of extension in the Pioneer metamorphic core complex with implications for the spatial-temporal pattern of Cenozoic extension and exhumation in the northern U.S. Cordillera, *Tectonics*, *31*, TC1008, doi:10.1029/2011TC002981.

1. Introduction

[2] Metamorphic core complexes have been recognized for more than thirty years as important features of syn- and post-orogenic, large-magnitude extensional strain [e.g., *Crittenden et al.*, 1980]. In the western North American Cordillera, core complexes formed throughout the Cenozoic in the orogenic hinterland (Figure 1). Core complexes from British Columbia (Canada) to north-central Idaho (U.S.A.) record initial extension in the Early Eocene immediately following, or perhaps during, the last stages of regional shortening (ca. 55–53 Ma) [e.g., *Ewing*, 1980; *Tempelman-Kluit and Parkinson*, 1986; *Brown and Journeay*, 1987; *Parrish et al.*, 1988; *Harms and Price*, 1992; *Foster et al.*, 2001, 2007; *Teyssier et al.*, 2005; *Carr and Simony*, 2006; *Hinchey et al.*, 2006; *Kruckenberg et al.*, 2008]. In contrast, data from core complexes between the Snake River plain and central Nevada indicate that they largely developed episodically starting at about 40 Ma and continuing into the Miocene [e.g., *Saltzer and Hodges*, 1988; *McGrew and Snee*, 1994; *MacCready et al.*, 1997; *Miller et al.*, 1999; *Mueller et al.*, 1999, *Wells et al.*, 2000; *Colgan et al.*, 2010; *Gans et al.*, 2011]. The Pioneer core complex (PCC) in

[1]Department of Geological Sciences, University of Florida, Gainesville, Florida, USA.
[2]Research School of Earth Sciences, Australian National University, Canberra, ACT, Australia.
[3]Department of Geosciences, Idaho State University, Pocatello, Idaho, USA.
[4]Formerly at Department of Geosciences, Idaho State University, Pocatello, Idaho, USA.
[5]Now at Department of Earth and Planetary Sciences, University of Tennessee, Knoxville, Tennessee, USA.

0278-7407/12/2011TC002981

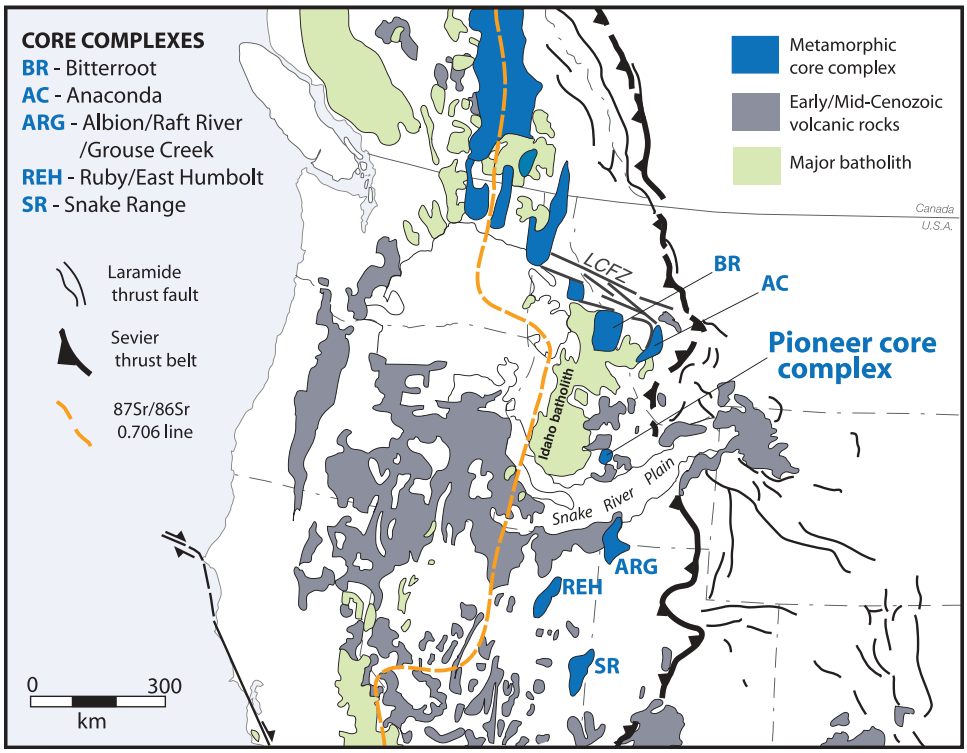

Figure 1. Map showing the location of the Pioneer core complex with respect to other core complexes and tectonic elements in the western Cordillera. Modified from *Foster et al.* [2007].

south-central Idaho (Figure 1) lies between these two core complex domains and therefore represents a key area for resolving the spatial-temporal patterns of core-complex development, which is a necessary first step in understanding the geodynamic processes involved in the change from contraction to extension, and relationship of large-magnitude extension to plate kinematics, boundary forces, and mantle upwelling.

[3] Previous work regarding the timing and directions of extension in the footwall and along the bounding detachment of the PCC is ambiguous. *Wust* [1986] conservatively constrained WNW-directed extensional motion on the bounding detachment as younger than ~48 Ma, while *Pavlis and O'Neill* [1987] argued that this motion was synchronous with ~48 Ma intrusions. In contrast, *Silverberg* [1990] suggested that SSW-directed extension occurred during intrusion of an ~48 Ma granodiorite sheet and that WNW-directed motion on the detachment occurred at 38–33 Ma. Of significance is the fact that upper crustal normal faults and dikes in the region largely record NW-SE extension during eruption of Challis volcanics at 50–45 Ma [*Dover*, 1981, 1983; *Janecke*, 1992; *Snider*, 1995; *Janecke et al.*, 1997]. Thus, the conclusions of *Silverberg* [1990] would require decoupling of the upper crust with orthogonally extending crust at different levels. These ambiguities are reflected in the different extension directions and widely varying ages of extension quoted for the PCC in compilations of the Cordilleran core complexes [e.g., *Sterne and Constenius*, 1997; *Dickinson*, 2002; *Bendick and Baldwin*, 2009].

[4] Constraining the timing of strain, metamorphism, and magmatism in the footwall is essential to understanding the mechanics of core-complex development. The kinematics and timing of footwall strain are particularly important in understanding the early strain history, the total amount of extensional strain, and the extent of coupling/decoupling between the upper and middle crust. Furthermore, documentation of the spatial variations in the age of core-complex initiation and rates/duration of extension is critical to understanding the geodynamic processes responsible for the switch from shortening to extension and for defining and understanding the mechanical/kinematic significance of extensional domain boundaries. The age of high-grade metamorphism, migmatization, penetrative strain fabrics, and large-scale doming in the footwall of the PCC is poorly resolved in the literature. These features have been attributed to Cretaceous shortening [*Dover*, 1981; *Silverberg*, 1990]. However, the fact that voluminous Eocene intrusions provide a potential heat source for melting/metamorphism, and because fabrics in an apparently Eocene granitic body wrap around the dome raise doubts about these interpretations. Previous interpretations attributing footwall strain to Late Cretaceous events are based on K-Ar and $^{40}Ar/^{39}Ar$ ages that now appear to be inaccurate due to excess argon, based on the U-Pb zircon results presented herein.

[5] In this contribution we provide new structural observations and U-Pb geochronology that provide a better understanding of the development of the PCC. These results establish the timing and directions of extension, as well as the distribution of extensional strain fabrics and age of high-grade metamorphism. We provide conclusive evidence that pervasive Early to Middle Eocene WNW-directed extensional strain was synchronous with emplacement of thick magmatic sheets and smaller dikes. We also show that

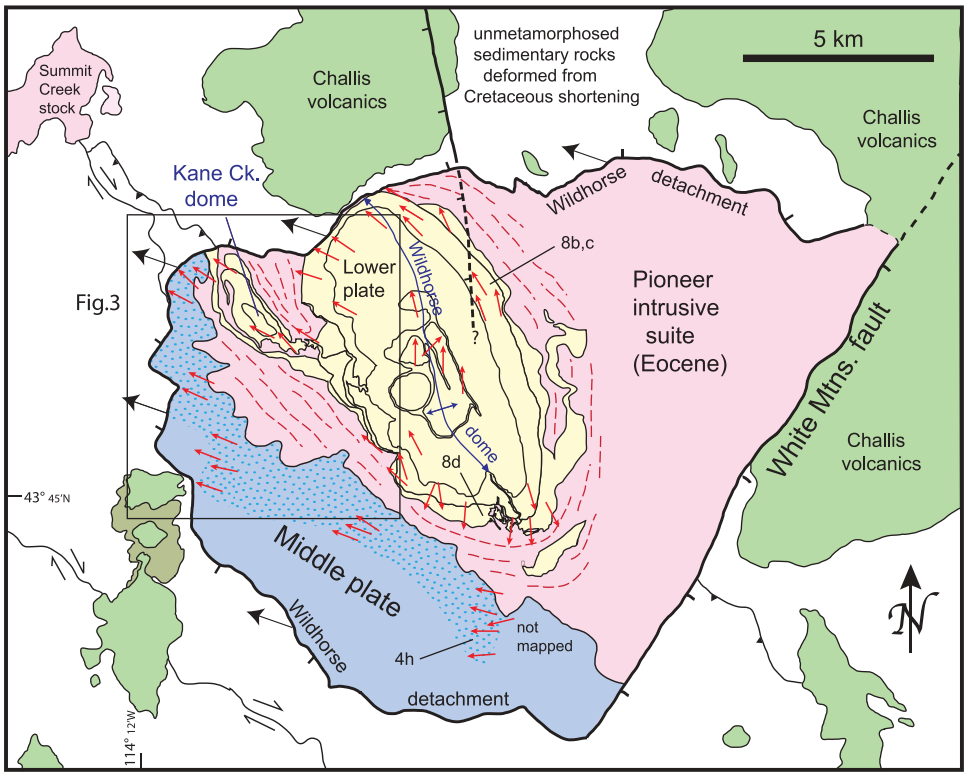

Figure 2. Simplified map of the Pioneer core complex with location map for study area shown in Figure 3. Red arrows show general stretching lineation trends for various regions that are discussed further in the text. Red dashed lines are foliation trajectories in PIS. Blue stipple indicates areas of pervasively developed W- to WNW lineation within Middle plate. Also shown are locations of photos/samples in Figures 4e, 8b, 8c, 8d, and 8e. Modified from *Dover* [1983] and *Wust* [1986].

much of the penetrative strain within the footwall is Eocene rather than Cretaceous, but that footwall strain patterns are complex. The implications of the timing and rates of extensional exhumation are discussed in the context of regional spatial-temporal patterns of core-complex development.

2. Regional Tectonic Setting

[6] The PCC occurs in the hinterland of the Sevier orogenic belt that resulted from Cretaceous to Paleogene retroarc thrusting and folding. The PCC lies between the Atlanta lobe of the Cretaceous Idaho batholith to the west and the foreland fold-thrust belt to the east. Relationships between sedimentary deposits, thrust faults, and normal faults in the fold-thrust belt to the east suggest that the transition from regional shortening to extension occurred relatively rapidly in Early Eocene time [*Constenius*, 1996]. In the PCC region, 50–45 Ma Challis volcanic and plutonic rocks unconformably overlie and intrude, respectively, deformed Paleozoic rocks. The Challis volcanics erupted during regional NW-SE extension [*Bennett*, 1986; *Janecke*, 1992; *Janecke et al.*, 1997].

[7] Regional extension following the cessation of shortening resulted in the development of a series of Cordilleran metamorphic core complexes exposed along the axis of the orogenic hinterland. The PCC is separated from the Bitterroot and Anaconda core complexes to the north by NE-trending faults of the Trans-Challis fault system [*Bennett*, 1986]. The Snake River plain separates the PCC from the Albion-Raft River-Grouse Creek core complexes to the south (Figure 1).

3. Overview of the Pioneer Core Complex

[8] Upper crustal rocks are juxtaposed with metamorphic rocks and Eocene granitoids along the curviplanar, brittle-ductile Wildhorse detachment system (Figure 2) [*Wust*, 1986; *O'Neill and Pavlis*, 1988; *Silverberg*, 1990; *Diedesch*, 2011] and along the NE-trending high-angle White Mountains fault in the southeast [*Dover*, 1983]. The Upper plate comprises unmetamorphosed Paleozoic sedimentary rocks that were folded and faulted during Cretaceous shortening and are unconformably overlain by Eocene (50–45 Ma) Challis volcanic rocks and intruded by syn-Challis plutons (Figure 2) [*Dover*, 1981, 1983].

[9] The footwall of the PCC was divided into a Middle and Lower plate by *Silverberg* [1990]. The Middle plate comprises a W- to SW-dipping panel of quartzite, marble, calc-silicate, and metapelite (Figures 2 and 3) that were referred to as the East Fork and Hyndman Groups by *Dover* [1981, 1983]. Protolith ages are constrained by single Ordovician fossil [*Dover*, 1983] and the presence of detrital zircons as young as 1.0 Ga in quartzite and calc-silicate lithologies [*Link et al.*, 2010]. In the northwestern part of the Middle plate, the structural section is duplicated by two apparent thrust faults (Figure 3) [*Dover*, 1983]. One shallow-dipping apparent extensional fault omits section in the same

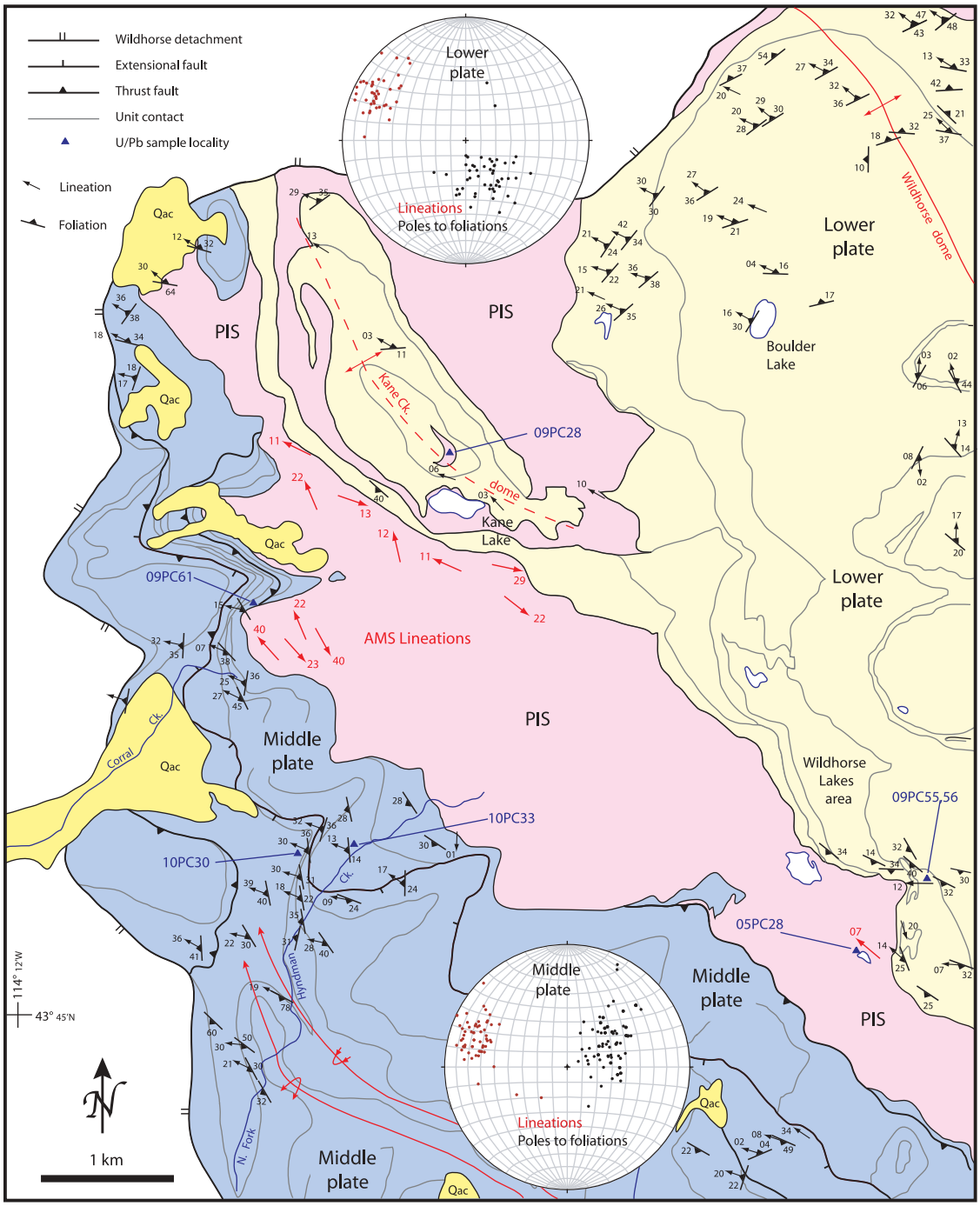

Figure 3. Geologic map of northwest part of the Pioneer core complex. Stereonets show structural data for northwestern section of Middle plate and Kane and Boulder Lakes area of Lower Plate. Black dots are poles to foliations and red dots are stretching lineations. Solid yellow pattern labeled Qac is Quaternary alluvium and colluvium. Red arrows are AMS lineations. Modified from *Dover* [1983].

area. This fault is semi-concordant with structural fabrics described in section 4.1.

[10] At the base of the Middle plate where it overlies and is intruded by the PIS, these rocks attained sillimanite grade metamorphic conditions [*Silverberg*, 1990]. Andalusite-bearing assemblages with sillimanite+muscovite upgrade in the contact aureole, indicate pressures in the upper part of the andalusite stability field [*Carmichael*, 1978; *Pattison and Tracy*, 1991]. Thus, the base of the middle plate was at ~11–15 km depth during emplacement of the PIS (aluminosilicate triple point of *Pattison* [1992]). The grade of Cretaceous regional metamorphism is difficult to discern, but is likely to have been greenschist grade. Folds and foliations in the Middle plate (outside of a 5-m zone adjacent to the PIS) were interpreted to have formed during Cretaceous regional shortening [*Dover*, 1983; *Silverberg*, 1990]. Although Cretaceous

structures undoubtedly developed in the Middle plate, our study indicates that vast areas of the Middle plate were also penetratively strained during Eocene extension.

[11] The Lower plate (Wildhorse gneiss complex of *Dover* [1981, 1983]) comprises a variety of Precambrian gneisses that include ca. 2.6 Ga and ~695 Ma orthogneiss, as well as possible metamorphosed Lemhi Group and other Meso-/Neoproterozoic paragneisses [*Durk*, 2007; *Link et al.*, 2007, 2010; *Cameron*, 2010]. Protolith age constraints suggest possible thrust duplication in the Lower plate [*Link et al.*, 2010]. The Lower plate contains abundant injections of granitic material and evidence for in situ melt. Metapelitic rocks, although not abundant, contain sillimanite and K-feldspar. Previous workers have interpreted the pervasive strain, high-grade metamorphism, and partial melt in the lower plate to result from Cretaceous shortening [*Dover*, 1983; *Silverberg*, 1990]. *Silverberg* [1990] suggested a pre-79 Ma age for the high-grade metamorphism on the basis of the high-temperature step ages in a hornblende $^{40}Ar/^{39}Ar$ spectrum.

[12] The Pioneer intrusive suite (PIS) comprises granitoids ranging from pyroxenite and diorite to granite [e.g., *Dover*, 1981; *Silverberg*, 1990]. The PIS has previously been broadly divided into two main units with poorly defined contacts: a western granodiorite sheet separating the Middle and Lower plates and a large, stock-like quartz monzonite body dominating the eastern half of the PCC footwall [*Dover*, 1983]. Prior to our work, the age of the PIS was constrained by only two cited U-Pb dates: (1) an unpublished U-Pb lower intercept age of 48.3 ± 0.6 Ma [*Dover*, 1981] from the eastern quartz monzonite and (2) a U-Pb zircon age of 49.0 ± 0.4 Ma from a small syenite body (P. K. Link and C. M. Fanning, unpublished data, 2006). A K-Ar hornblende age of ~68 Ma [*Dover*, 1983] for the western granodiorite led *O'Neill and Pavlis* [1988] to the conclusion that foliations in the western sheet are Cretaceous in age.

[13] The map-scale structural geometry of the Lower plate is dominated by the elongate NNW-trending Wildhorse dome [*Dover*, 1983], which is defined by unit contacts and metamorphic layering of the Lower plate, as well as by foliations in the PIS. The smaller, more poorly defined Kane Creek dome occurs in the northwest part of the footwall [*Dover*, 1983]. Dips on the southwest flank of the Wildhorse dome are moderate, whereas the northeast flank is locally subvertical to overturned. Foliations in the PIS flanking the dome follow the outline of the dome, suggesting that doming occurred after emplacement of at least some phases of the PIS and therefore occurred in the Eocene.

[14] The Middle-/Lower plate boundary was interpreted by *Silverberg* [1990] as a down-to-the-SSW shear zone (which he termed the Hyndman shear zone) that was active during emplacement of the western PIS sheet, which he assumed to be Eocene. The Wildhorse detachment cuts across the PIS, as well as the Middle and Lower plates and dips moderately north along the northern section and west or southwest along the southwest extent [*Wust*, 1986; *O'Neill and Pavlis*, 1988; *Silverberg*, 1990; *Diedesch*, 2011]. Brittle fabrics within the fault zone overprint mylonites in the northwestern half of the core complex. Micas within the Wildhorse detachment zone and throughout the footwall give $^{40}Ar/^{39}Ar$ ages of 38–35 Ma and low-temperature steps from K-feldspar are ~33 Ma [*Silverberg*, 1990]. Thus, *Silverberg* [1990] proposed a two-stage model for extension within the PCC: (1) syn-magmatic, SSW-down motion along the Hyndman shear zone at ca. 48 Ma, followed by (2) top-WNW motion on the Wildhorse detachment at ~38–33 Ma.

4. Footwall Strain Within the PCC

[15] Several key areas reveal important relationships that allow timing and kinematics of the strain to be deciphered. Here, we focus largely on the northwest corner of the PCC, across a structural section through the Middle and Lower plates, as well as the intervening PIS sheet (Figure 3). We describe the structures of the footwall with focus on outcrop-scale strain features and relationships with granitic dikes in the Middle and Lower plates and plutonic phases of the PIS. We discuss the youngest set of penetrative fabrics. This extensional strain is denoted as D_{2E} to indicate that it may locally overprint earlier fabrics and is extensional in origin. U-Pb geochronologic data presented in subsequent sections, indicate that D_{2E} occurred in the Eocene. We use D_1 here to encompass any earlier formed fabrics, most of which presumably formed from Mesozoic shortening.

4.1. Middle Plate

[16] Mesoscopically, calc-silicates, impure layered marbles, and quartzites are dominated by a compositional layering and mineral alignment that is generally parallel to lithologic contacts. Mesoscopic isoclinal and locally intrafolial folds are present locally within the section. Stretching lineations trend west to west-northwest (Figure 3) and are defined by elongate quartz, mica smears, amphibole, and mm-scale siliceous stringers in marbles. In banded calc-silicate, a prominent lineation appears to have formed from intersection of folded mm-scale and finer bands that intersect the dominant axial surface. Although there is some scatter, these intersection lineations generally have west-northwest trends, parallel to stretching lineations. Locally, elongate minerals are poorly aligned suggesting that metamorphic mineral growth outlasted penetrative strain in parts of the section.

[17] In the North Fork Hyndman Creek valley, an isoclinal anticline-syncline fold pair with a northeast vergence is defined by the Kinnikinik quartzite (Figure 3). The anticline fold hinge plunges shallowly west-northwest, parallel to the stretching lineation.

[18] Felsic dikes (bt-granite, pegmatite, and aplite) are common within the northwest portion of the Middle plate and show a range of timing relationships with the structural fabrics. One of the striking features of the Middle plate is the abundance of relatively planar dikes that sharply cut the compositional layering (Figures 4a–4c), especially in the deeper parts of the section. These crosscutting dikes dominate the views of many of the ridges in the northwest part of the map area (Figure 4a). Other dikes, however, are isoclinally folded and/or stretched into isolated boudins (Figures 4c–4f). Furthermore, some dikes show planar, sharply crosscutting segments that deflect into segments that are thinned and/or boudinaged and make a lower angle with respect to the dominant layering. Several cliff faces show the full range of timing relationships between D_{2E} and the granitic dikes (Figure 4c). In some deformed granitic dikes, a WNW-trending lineation parallel to the enclosing metamorphic rocks, is visible.

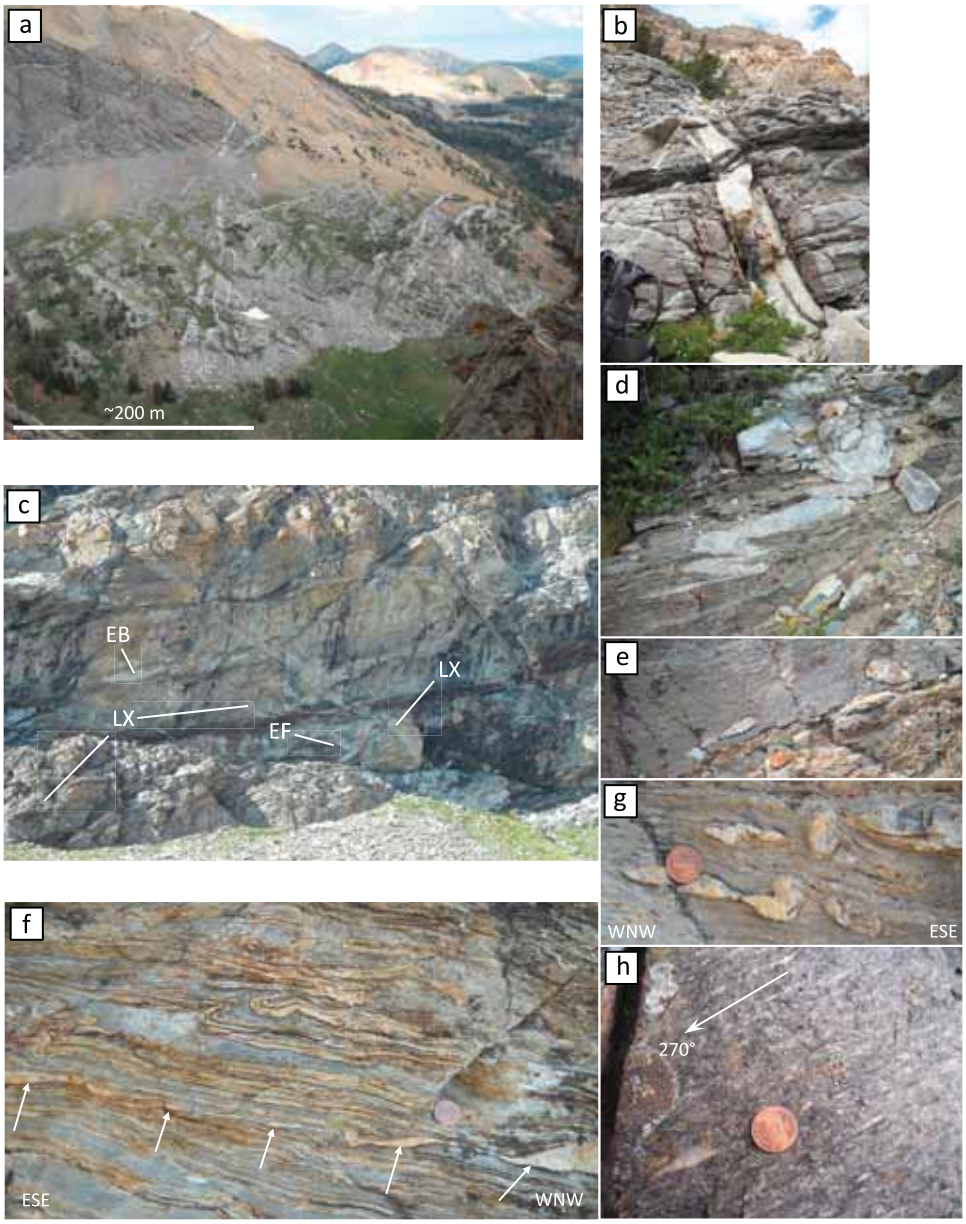

Figure 4. Field photos of structural features in Middle plate. (a) Suite of steep N- to NW-striking granitic dikes that crosscut Eocene D_{2E} fabric in Middle plate. View looking toward SSE across the upper part of North Fork Hyndman Ck. (b) Crosscutting dike dated as 45.9 ± 0.3 Ma (sample 10PC33). See Figure 3 for location and Figure 7c for U-Pb age information. Dike is ~0.5 m across in lower part. View looking toward NW. (c) Cliff face in lower part of Middle plate showing a range of timing relationships between granitic dikes (light-colored) and D_{2E} strain. EB, early dike that is transposed and boudinaged; EF, early tightly folded dike; LX, late crosscutting dikes. Cliff face is ~70–80 m high. View is looking toward NNW. Location is in the upper part of North Fork Hyndman Creek. (d) Highly strained and isoclinally folded leucogranite dike from the base of the Middle plate. See Figure 3 for location and Figure 7a for U-Pb age information (sample 09PC61). View is ~3 m across and looking toward the NW. (e) Leucogranite boudins in Saturday Mountain Fm. on the ridge west of the upper part of North Fork Hyndman Creek. Leucogranite (sample 10PC30) yields zircons with a weighted mean age of 45.7 ± 0.8 Ma (Figure 7b) (f) Eocene mesoscopic structures in Saturday Mountain Fm. of Middle plate. Shows asymmetrically boudinaged oblique granitic layer with top-WNW shear sense. Arrows show boudin train of granitic layer that cuts across layering at low angle. Also shows abundant WNW-vergent asymmetric folds of original layering. Outcrop is on the ridge west of the upper part of North Fork Hyndman Creek. (g) Rotated and folded granitic clasts in Saturday Mountain Fm. showing top-WNW shear sense. Outcrop is on the ridge west of the upper part of North Fork Hyndman Creek. (h) Coarse sillimanite defining W-trending lineation in moderately SSW-dipping pelitic schist from southern area of Middle plate. Location shown in Figure 2.

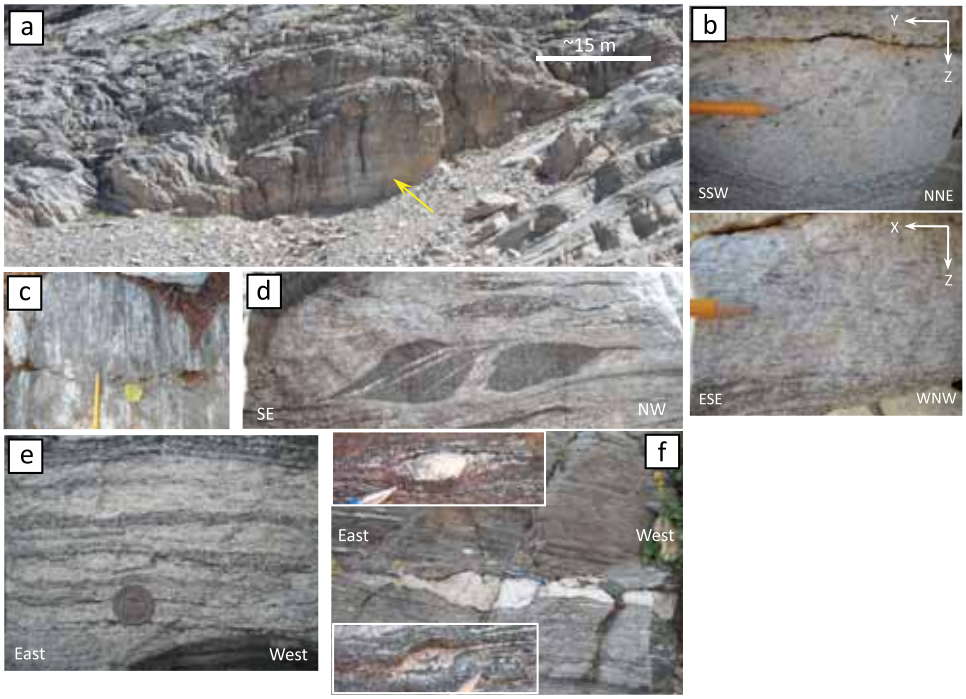

Figure 5. Field photos of structural features in the Lower plate. (a) Isoclinal folds (indicated by yellow arrow) of leucocratic dike within Archean felsic gneiss. View looking toward NNE. Outcrop in Boulder Lake area. (b) Mutually perpendicular faces of strained leucogranite layer in Boulder Lake area. YZ face shows minimal fabric and XZ section shows prominent fabric. This relationship indicates prominent WNW-trending lineation. (c) Prominent WNW-trending lineation in Kane Creek. Pencil points toward WNW. (d) Asymmetric tails on mafic boudin indicating top-WNW shear. Outcrop in Kane Lake area. View is ~0.5 m across. (e) Interlayered meta-psammite and highly strained Eocene leucogranite. See Figure 3 for location and Figure 8a for U-Pb age data (sample 09PC56). (f) Boudins of Eocene leucogranite in highly strained biotite-rich meta-psammite. See Tables 1a and 1b and text for age U-Pb age information (sample 09PC55). Insets are close-ups of clasts with asymmetric tails showing top-W shear sense (pen and pencil tips for scale). Outcrop in Wildhorse Lakes area. See Figure 3 for location.

[19] Shear-sense indicators viewed on lineation-parallel, foliation-normal faces yield a consistent top-WNW sense. These include asymmetric, sheared boudins, rotated clasts, continuous trains of asymmetric folds, and sheared-out fold hinges (Figures 4f and 4g). Taken together, the described relationships indicate that top-WNW strain is pervasive and occurred during and/or after emplacement of granitic dikes, but largely ceased before the final stages of injection. This is consistent with the presence of locally randomly oriented metamorphic minerals. Kinematically and geometrically identical lower temperature mylonitic fabrics occur upsection along the Wildhorse detachment in the northwest apex of the core complex [*Wust*, 1986; *O'Neill and Pavlis*, 1988; *Silverberg*, 1990; this study]. However, post-mylonitic cross-cutting dikes have not been found in these areas.

[20] In the Corral Creek area of the northwest part of the core complex (Figure 3), D_{2E} fabrics span the entire section between the Wildhorse detachment and PIS. To the south, the D_{2E} strain diverges from the Wildhorse detachment and follows the upper contact of the western PIS granodiorite sheet (Figure 2). The D_{2E} strain has been mapped in the deeper parts of the Middle plate (Figures 2–4), where it is delineated locally by transposed dikes and a WNW- to W- trending lineation, including coarse sillimanite (Figure 4h). In the southern areas, higher levels within the Middle plate appear to be relatively unaffected by D_{2E}, as indicated by the lack of a lineation and the preservation of cross-bedding in some of the quartzites.

4.2. Lower Plate

[21] Observations from the Lower plate in the Boulder Lake area reveal kinematic characteristics and relationships with granitic material that are similar to those described in the Middle plate. Here, on the northwest flank of the dome, *ca.* 2.6 Ga felsic gneisses [*Durk*, 2007; *Link et al.*, 2010] contains a W- to NW-dipping foliation that is accentuated by transposed layers of more leucocratic material, which locally define isoclinal folds over a range of scales (Figure 5a). A WNW-trending lineation (Figure 3) is defined by biotite smears and elongate quartz and feldspar (Figure 5b). Locally, these fabrics are sharply crosscut by segments of granitic dikes. Higher in the section to the west and northwest, in closer proximity to the Wildhorse detachment, mylonitic zones highlighted by porphyroclastic textures and grain-size reduction with the same WNW-trending lineation orientation become more common.

[22] WNW-trending lineations are well-developed in gneiss of the Lower plate in the Kane Creek area (Figures 3 and 5c). Fabrics with $L \gg S$ are common and lineations are

Figure 6. Field photos of structural features of the Pioneer intrusive suite. (a) Photo of western granodiorite sheet showing prominent foliation highlighted by elongate enclaves. Also shown are largely post-kinematic leucocratic dikes cutting foliation. Outcrop in Kane Lake area. (b) Close-up photo of typical homogeneous, magmatic foliation in western granodiorite phase of the PIS. Outcrop in Kane Creek area. (c) Domino-style mafic boudins rotated and sheared into asymmetric forms. Inferred shear-sense is top-NW. Inset shows other part of boudin train displaying minimal rotation. Outcrop is in Kane Lake area within 30 m of Figure 5d, which also shows top-NW shear sense in adjacent Lower plate gneiss. Hammer is ~37 cm long.

parallel to hinges of folds with variable inclination and tightness, perhaps indicators of more constrictional strain in this area (Figure 5c). Shear-sense indicators indicate top-WNW motion (Figure 5d).

[23] In the Wildhorse Lakes area (Figure 3), a shallowly SW-dipping section of semi-pelite, meta-psammite, quartzite, and calc-silicate occurs on the west flank of the dome. Granitic material occurs as boudins and highly strained layers transposed into parallelism with the foliation (Figures 5e and 5f). Lineations are poorly developed here, but calc-silicate boudins have N-S axes indicating roughly E-W stretching. Adjacent metasedimentary rocks display abundant low-strain, W-vergent folds and porphyroclastic remnants of highly strained granitic material show distinct asymmetric wings and tails indicating top-west shear (Figure 5f).

[24] Other Lower plate domains around the Wildhorse dome have different lineation orientations. For example, the northeast flank of the dome has gently plunging NNW-SSE lineations and the southern part of the dome displays S- to SSW-plunging lineations (Figure 2). The strain in these areas also involves granitic dikes and show similar temporal relationships as described above in other areas. This suggests that these fabrics are also Eocene in age and formed during regional extension. The domains of varying lineation orientations may result from modifications of pre-existing fabrics during doming or from deeper level decoupled flow. The kinematics of the Lower plate strain and doming are still somewhat unclear, but are the focus of ongoing studies. However, it seems clear that the fabric pattern cannot be ascribed to the simple case of passive folding of an originally WNW-trending lineation.

4.3. Pioneer Intrusive Suite (PIS)

[25] Structural observations from the PIS in the northwest corner of the PCC come primarily from the two intrusive units in the Kane Creek drainage: a volumetrically dominant coarse-grained hornblende biotite granodiorite and a sill of porphyritic biotite granite. Both units show a homogeneous foliation defined by aligned biotite, hbl-bt aggregates, and feldspars, as well as by elongate mafic enclaves (Figures 6a and 6b). Petrographic observations commonly show only minor evidence for solid-state deformation of quartz and a distinct alignment of subhedral feldspars, indicating foliation formation in a dominantly magmatic state. These foliations are parallel to the high-temperature foliations in the enclosing metamorphic rocks. An increase in the intensity of solid-state strain fabrics within the PIS near its upper and lower contacts was not observed.

[26] Macroscopic lineations in the PIS were discernible in the field in only a few locations where they trend NW. Magnetic lineations measured through the anisotropy of magnetic susceptibility (AMS) consistently trend WNW-ESE to NNW-SSE in the Kane Lake area (Figure 3) [*Kent et al.*, 2010], parallel to lineations in the adjacent Middle and Lower plates. Rare shear-sense indicators, such as the rotated dominoes sheared into asymmetric boudins shown

Table 1a. Summary of SHRIMP U-Pb Zircon Results

							Total Ratios						Age	
Grain Spot	U (ppm)	Th (ppm)	Th/U	$^{206}Pb^*$ (ppm)	$^{204}Pb/^{206}Pb$	f_{206} (%)	$^{238}U/^{206}Pb$	$^{238}U/^{206}Pb$ 2σ Plus/Minus	$^{207}Pb/^{206}Pb$	$^{207}Pb/^{206}Pb$ 2σ Plus/Minus	$^{206}Pb/^{238}U$	$^{206}Pb/^{238}U$ 2σ Plus/Minus	$^{206}Pb/^{238}U$	2σ Plus/Minus
							09PC61							
1.1	383	255	0.665	2.4	0.000967	0.39	137.3	2.0	0.0501	0.0024	0.0073	0.0001	46.6	1.4
3.1	5643	630	0.112	38.8	0.000038	0.07	125.0	1.3	0.0476	0.0004	0.0080	0.0001	51.3	1.1
6.1	454	17	0.036	3.0	-	<0.01	131.3	1.8	0.0464	0.0015	0.0076	0.0001	48.9	1.4
7.1	4140	149	0.036	33.4	-	0.03	106.4	1.1	0.0474	0.0004	0.0094	0.0001	60.3	1.3
8.1	702	21	0.031	4.5	0.000933	0.36	134.3	1.7	0.0498	0.0012	0.0074	0.0001	47.7	1.2
10	207	103	0.497	1.3	0.001723	1.02	135.1	2.4	0.0551	0.0024	0.0073	0.0001	47.1	1.7
11	1639	74	0.045	10.6	-	<0.01	133.3	1.5	0.0469	0.0008	0.0075	0.0001	48.2	1.1
12	519	11	0.021	3.6	0.000248	0.22	124.6	1.7	0.0488	0.0014	0.0080	0.0001	51.4	1.4
17	192	84	0.438	1.2	0.002439	0.47	136.5	2.5	0.0507	0.0029	0.0073	0.0001	46.8	1.7
							10PC33							
1.1	6307	3169	0.502	43.0	0.000083	0.25	126.1	1.3	0.0490	0.0003	0.0079	0.0001	50.8	1.0
1.2	1405	380	0.270	8.6	-	0.11	140.0	1.5	0.0478	0.0007	0.0071	0.0001	45.8	1.0
2.1	5358	455	0.085	35.0	-	0.07	131.5	1.3	0.0476	0.0003	0.0076	0.0001	48.8	1.0
2.2	1058	569	0.538	6.4	0.000127	0.10	143.0	1.7	0.0477	0.0008	0.0070	0.0001	44.9	1.1
3.1	4908	2465	0.502	30.6	0.000229	0.07	137.6	1.4	0.0475	0.0004	0.0073	0.0001	46.6	1.0
4.1	637	97	0.152	4.2	0.000166	0.32	131.5	1.5	0.0495	0.0011	0.0076	0.0001	48.7	1.1
4.2	3637	1685	0.463	24.2	0.000100	0.13	129.1	1.3	0.0480	0.0005	0.0077	0.0001	49.7	1.0
5.1	2183	1023	0.469	13.6	0.000313	0.03	137.4	1.4	0.0472	0.0006	0.0073	0.0001	46.7	1.0
6.1	505	299	0.592	3.2	0.000347	0.42	135.6	1.6	0.0503	0.0013	0.0073	0.0001	47.2	1.1
6.2	633	404	0.638	3.8	0.000349	<0.01	141.9	1.6	0.0465	0.0011	0.0070	0.0001	45.3	1.1
7.1	4343	1842	0.424	29.2	0.000128	0.18	127.9	1.3	0.0484	0.0004	0.0078	0.0001	50.1	1.0
7.2	930	470	0.506	5.8	0.000670	0.91	138.4	1.5	0.0542	0.0010	0.0072	0.0001	46.0	1.0
8.1	1112	943	0.848	7.0	0.000253	0.06	137.2	2.2	0.0474	0.0009	0.0073	0.0001	46.8	1.5
9.1	717	198	0.277	4.4	-	0.18	141.0	1.6	0.0483	0.0010	0.0071	0.0001	45.5	1.1
10	496	341	0.689	3.1	0.000395	0.16	139.1	1.6	0.0482	0.0012	0.0072	0.0001	46.1	1.1
11	3797	1506	0.397	23.6	0.000090	0.07	138.3	1.4	0.0475	0.0004	0.0072	0.0001	46.4	1.0
11	1087	492	0.453	6.6	0.000158	0.04	141.2	1.6	0.0473	0.0008	0.0071	0.0001	45.5	1.0
12	978	531	0.543	6.0	0.000061	<0.01	141.0	1.6	0.0469	0.0008	0.0071	0.0001	45.6	1.0
13	467	291	0.624	2.8	0.002489	0.45	142.1	2.6	0.0505	0.0019	0.0070	0.0001	45.0	1.6
14	726	246	0.338	4.4	0.000314	<0.01	140.4	1.6	0.0463	0.0010	0.0071	0.0001	45.8	1.0
15	301	163	0.543	1.9	0.001513	0.55	138.5	1.7	0.0513	0.0016	0.0072	0.0001	46.1	1.2
16	416	271	0.652	2.5	-	0.12	140.6	2.3	0.0479	0.0014	0.0071	0.0001	45.6	1.5
17	3258	1949	0.598	20.2	0.000050	0.16	138.5	1.4	0.0482	0.0005	0.0072	0.0001	46.3	1.0
18	3270	2163	0.662	20.4	0.000044	<0.01	137.8	1.5	0.0462	0.0005	0.0073	0.0001	46.6	1.0
19	3244	2617	0.807	20.0	0.000043	0.08	139.2	1.5	0.0476	0.0006	0.0072	0.0001	46.1	1.0
20	5919	3209	0.542	38.7	0.000209	0.22	131.4	1.4	0.0487	0.0004	0.0076	0.0001	48.8	1.1
21	607	302	0.497	3.6	0.003885	<0.01	143.3	2.0	0.0460	0.0011	0.0070	0.0001	44.9	1.3
22	709	721	1.017	4.2	0.000259	<0.01	143.8	1.7	0.0467	0.0010	0.0070	0.0001	44.7	1.0
							09PC55							
17	231	29	0.126	1.5	0.000649	0.33	136.0	2.3	0.0496	0.0022	0.0073	0.0001	47.1	1.6
3.1	257	0	0.001	1.9	0.000018	0.45	116.7	1.9	0.0507	0.0022	0.0085	0.0001	54.8	1.8
21	1203	2	0.002	9.2	-	<0.01	112.1	1.3	0.0461	0.0008	0.0089	0.0001	57.3	1.3
23	190	0	0.001	1.5	0.001374	0.37	106.7	1.8	0.0501	0.0022	0.0093	0.0002	59.9	2.1
15	270	2	0.006	2.2	0.000675	1.38	105.3	1.6	0.0582	0.0019	0.0094	0.0001	60.1	1.8
8.1	510	3	0.006	4.2	0.000122	2.03	103.4	1.3	0.0633	0.0015	0.0095	0.0001	60.8	1.6
							09PC15							
1.1	2267	17	0.007	15.0	0.000338	0.05	130.0	1.4	0.0474	0.0007	0.0077	0.0001	49.4	1.1
2.1	4073	12	0.003	29.8	0.000098	0.07	117.5	1.2	0.0477	0.0005	0.0085	0.0001	54.6	1.2
2.2	3062	20	0.006	19.6	0.000150	0.12	134.5	1.5	0.0479	0.0007	0.0074	0.0001	47.7	1.0
3.1	3169	16	0.005	25.3	0.000525	1.02	107.4	1.5	0.0553	0.0006	0.0092	0.0001	59.1	1.6
3.2	913	12	0.014	6.0	0.000206	0.12	131.8	1.6	0.0479	0.0011	0.0076	0.0001	48.7	1.2
4.1	652	5	0.008	4.3	0.000071	0.16	130.5	1.7	0.0482	0.0013	0.0076	0.0001	49.1	1.3
5.1	486	9	0.018	3.3	0.001373	0.49	127.5	1.7	0.0509	0.0015	0.0078	0.0001	50.1	1.4
6.1	713	7	0.010	4.8	0.000424	<0.01	128.0	1.6	0.0468	0.0012	0.0078	0.0001	50.2	1.3
7.1	318	7	0.021	2.1	0.001494	0.20	129.7	2.0	0.0486	0.0018	0.0077	0.0001	49.4	1.5
8.1	301	5	0.016	2.0	0.002682	1.26	129.4	2.1	0.0570	0.0022	0.0076	0.0001	49.0	1.6
9.1	535	5	0.009	3.9	0.000808	0.41	118.9	1.6	0.0503	0.0014	0.0084	0.0001	53.8	1.4
10	631	9	0.014	4.0	0.000655	0.81	134.1	1.8	0.0534	0.0021	0.0074	0.0001	47.5	1.3
11	1488	10	0.006	10.7	0.000390	0.25	119.9	1.4	0.0491	0.0011	0.0083	0.0001	53.4	1.3
12	504	8	0.015	3.3	0.001049	0.39	131.6	1.9	0.0501	0.0017	0.0076	0.0001	48.6	1.4
13	1816	10	0.006	12.6	0.000471	0.14	123.6	1.4	0.0481	0.0008	0.0081	0.0001	51.9	1.2
14	1289	9	0.007	8.4	0.000562	0.06	131.9	3.7	0.0474	0.0011	0.0076	0.0002	48.7	2.8
16	1146	5	0.005	8.9	0.000314	0.24	110.4	1.4	0.0491	0.0013	0.0090	0.0001	58.0	1.4
17	381	6	0.015	2.6	0.000283	0.96	125.2	2.4	0.0546	0.002	0.0079	0.0002	50.8	2.0

Table 1a. (continued)

Grain Spot	U (ppm)	Th (ppm)	Th/U	$^{206}Pb^*$ (ppm)	$^{204}Pb/^{206}Pb$	f_{206} (%)	Total Ratios $^{238}U/^{206}Pb$	$^{238}U/^{206}Pb$ 2σ Plus/Minus	$^{207}Pb/^{206}Pb$	$^{207}Pb/^{206}Pb$ 2σ Plus/Minus	$^{206}Pb/^{238}U$	$^{206}Pb/^{238}U$ 2σ Plus/Minus	Age $^{206}Pb/^{238}U$	Age 2σ Plus/Minus
							05PC28							
1.1	654	209	0.319	4.2	0.000442	0.39	133.8	1.7	0.0500	0.0013	0.0074	0.0001	47.8	1.2
2.1	211	134	0.631	1.4	0.001405	0.32	130.1	2.1	0.0495	0.0023	0.0077	0.0001	49.2	1.6
3.1	219	115	0.527	1.4	0.000607	0.81	137.6	2.2	0.0534	0.0024	0.0072	0.0001	46.3	1.5
4.1	270	128	0.473	1.7	-	0.77	135.8	2.1	0.0531	0.0022	0.0073	0.0001	46.9	1.5
5.1	194	92	0.476	1.2	-	0.22	133.5	2.3	0.0487	0.0027	0.0075	0.0001	48.0	1.7
6.1	233	108	0.466	1.4	-	0.11	138.3	2.3	0.0478	0.0024	0.0072	0.0001	46.4	1.6
7.1	166	86	0.522	1.1	0.000413	0.11	133.2	2.3	0.0479	0.0025	0.0075	0.0001	48.2	1.7
8.1	268	136	0.506	1.8	0.000543	0.42	128.4	1.9	0.0503	0.0019	0.0078	0.0001	49.8	1.5
9.1	215	109	0.509	1.4	-	0.54	128.8	2.1	0.0513	0.0023	0.0077	0.0001	49.6	1.6
10	239	148	0.618	1.6	-	0.53	132.2	2.1	0.0512	0.0022	0.0075	0.0001	48.3	1.5
11	362	147	0.406	2.4	0.001200	0.21	130.6	1.8	0.0486	0.0018	0.0076	0.0001	49.1	1.4
12	168	82	0.490	1.1	0.001542	0.18	133.2	2.3	0.0484	0.0026	0.0075	0.0001	48.1	1.7
13	203	105	0.517	1.3	0.002603	0.56	132.2	2.3	0.0514	0.0028	0.0075	0.0001	48.3	1.7
14	210	109	0.517	1.4	0.000783	1.28	130.1	2.2	0.0571	0.0026	0.0076	0.0001	48.7	1.7
15	253	129	0.510	1.7	0.002569	2.66	130.6	2.1	0.0680	0.0026	0.0075	0.0001	47.9	1.6
16	324	153	0.474	2.1	0.000327	0.26	132.9	2.0	0.0491	0.0021	0.0075	0.0001	48.2	1.5
17	358	141	0.394	2.4	0.000775	0.07	130.7	1.8	0.0475	0.0016	0.0076	0.0001	49.1	1.3
18	760	718	0.945	5.1	0.000281	0.45	128.9	1.5	0.0506	0.0014	0.0077	0.0001	49.6	1.2
19	187	100	0.533	1.2	0.001305	0.61	134.1	2.1	0.0518	0.0022	0.0074	0.0001	47.6	1.5
20	273	103	0.377	1.9	0.001758	0.29	123.4	1.7	0.0493	0.0025	0.0081	0.0001	51.9	1.5
							09PC28							
1.1	1345	251	0.187	9.0	0.000103	0.03	129.0	1.4	0.0472	0.0008	0.0078	0.0001	49.8	1.1
2.1	1313	526	0.401	10.4	0.000199	0.75	108.3	1.2	0.0531	0.0008	0.0092	0.0001	58.8	1.3
3.1	1492	117	0.078	9.8	0.000085	0.29	130.5	1.5	0.0493	0.0008	0.0076	0.0001	49.1	1.1
4.1	453	149	0.328	2.9	0.000267	0.25	132.6	1.7	0.0490	0.0014	0.0075	0.0001	48.3	1.2
4.2	909	270	0.296	6.0	0.000538	0.31	129.9	1.5	0.0495	0.0010	0.0077	0.0001	49.3	1.1
5.1	2023	421	0.208	14.3	-	0.24	121.6	1.3	0.0489	0.0006	0.0082	0.0001	52.7	1.1
6.1	2332	61	0.026	16.5	0.000035	0.03	121.3	1.3	0.0473	0.0006	0.0082	0.0001	52.9	1.1
7.1	3482	126	0.036	24.0	0.000057	0.13	124.7	1.3	0.0481	0.0005	0.0080	0.0001	51.4	1.1
8.1	1273	49	0.039	8.4	0.000140	0.03	129.5	1.4	0.0473	0.0008	0.0077	0.0001	49.6	1.1
9.1	3265	329	0.101	22.5	-	<0.01	124.8	1.3	0.0470	0.0005	0.0080	0.0001	51.4	1.1
10	1237	308	0.249	8.2	0.000202	0.06	128.9	1.4	0.0475	0.0008	0.0078	0.0001	49.8	1.1
12	2486	565	0.227	17.8	0.000067	<0.01	120.1	1.3	0.0470	0.0005	0.0083	0.0001	53.5	1.1
13	1481	75	0.051	10.1	-	0.03	125.8	1.4	0.0473	0.0008	0.0079	0.0001	51.0	1.1
14	1664	75	0.045	11.2	0.000059	<0.01	127.8	1.4	0.0467	0.0007	0.0078	0.0001	50.3	1.1
15	1420	78	0.055	9.1	-	<0.01	133.7	1.5	0.0468	0.0008	0.0075	0.0001	48.1	1.1
16	3334	240	0.072	23.4	0.000040	<0.01	122.2	1.3	0.0468	0.0005	0.0082	0.0001	52.6	1.1
17	2060	77	0.038	14.4	0.000080	0.61	122.5	2.0	0.0519	0.0051	0.0081	0.0001	52.1	1.8
18	1091	88	0.081	7.1	0.000040	0.01	131.1	1.5	0.0471	0.0009	0.0076	0.0001	49.0	1.1
19	996	209	0.210	6.6	-	0.04	129.5	1.5	0.0473	0.0009	0.0077	0.0001	49.6	1.1
20	1028	572	0.557	6.8	0.000018	<0.01	129.7	1.5	0.0468	0.0009	0.0077	0.0001	49.5	1.1
21	5416	313	0.058	39.7	0.000033	0.08	117.1	1.2	0.0477	0.0003	0.0085	0.0001	54.8	1.1
22	5821	932	0.160	41.5	0.000054	<0.01	120.4	1.3	0.0469	0.0003	0.0083	0.0001	53.3	1.1

in Figure 6c, suggest top-NW shear during emplacement of the granodiorite. In most areas, relatively planar leucocratic dikes crosscut the homogeneous fabric of the PIS.

5. U-Pb Dating and the Timing of Footwall Strain

[27] The timing of D_{2E} top-WNW extensional strain is constrained by combining new U-Pb ages with structural relationships discussed above. All crystallization ages discussed here are from zircons analyzed on either the SHRIMP-II at the Australian National University (referred to here as SHRIMP) or on the laser ablation ICPMS at the University of Florida (referred to here as ICPMS). Age data are provided in Tables 1a and 1b and a summary of results and general sample information is provided in Table 2. Although all samples from small-scale intrusions in the Middle and Lower plate contain inherited grains ranging from Neoproterozoic (~1.1 Ga) to Neoarchean (~2.6 Ga), only Paleocene/Eocene ages are discussed in this section and shown in Tables 1a and 1b. Given the focus on these young grains, all ages discussed in text are $^{238}U/^{206}Pb$ ages. Weighted-mean plots are given for each sample; Terra-Wasserburg plots, age histograms, and a discussion of the analytical techniques are provided in the auxiliary material.[1] Sample locations are shown in Figures 2 and 3.

5.1. Middle Plate

[28] The lineated, isoclinally folded dike (sample 09PC61) from the base of the Middle plate shown in Figure 4d yielded eight Eocene grains ranging in age from 46.6 ± 0.7 to 51.4 ± 0.7 Ma (SHRIMP). The youngest four grains, all within 1σ error, yield an age of 47.1 ± 0.7 Ma (Figure 7a),

[1] Auxiliary materials are available in the HTML. doi:10.1029/2011TC002981.

Table 1b. Summary of ICPMS U-Pb Zircon Results

Grain Spot	Total Ratios $^{206}Pb/^{238}U$	Total Ratios 2σ Plus/Minus	Age $^{206}Pb/^{238}U$	Age 2σ Plus/Minus
		09PC56		
15	0.0076	0.0002	49.0	1.5
20	0.0076	0.0003	48.9	1.6
26	0.0075	0.0002	48.1	1.6
29	0.0077	0.0002	49.6	1.6
30	0.0076	0.0003	48.7	1.8
		05PCRM01		
1	0.0084	0.0003	54.1	4.4
10	0.0081	0.0003	52.0	4.2
12	0.0082	0.0003	52.5	4.3
13	0.0078	0.0003	49.9	4.2
20	0.0084	0.0003	53.7	4.3
22	0.0080	0.0003	51.6	4.2
23	0.0081	0.0003	52.0	4.1
26	0.0081	0.0004	52.1	5.1
		10PC30		
1	0.0070	0.0002	45.1	2.0
2	0.0069	0.0001	44.6	1.7
3	0.0073	0.0001	46.8	1.8
4	0.0072	0.0001	46.5	1.8
6	0.0073	0.0001	46.7	1.8
7	0.0069	0.0001	44.6	1.6
8	0.0068	0.0001	44.0	1.9
10	0.0073	0.0001	46.7	1.8
11	0.0070	0.0001	44.8	1.7
12	0.0080	0.0002	51.4	2.0
13	0.0069	0.0001	44.1	1.6
14	0.0071	0.0001	45.8	1.7
15	0.0078	0.0002	50.2	2.0
16	0.0072	0.0001	46.6	1.7
17	0.0077	0.0002	49.4	2.2
18	0.0067	0.0001	42.8	1.6
19	0.0072	0.0002	46.0	2.0
20	0.0074	0.0001	47.6	1.9

which represents the best estimate for the crystallization age of the dike. An age of 47.6 ± 0.8 Ma is obtained using the youngest six grains, all within 2σ error. Given the range of ages and the small number of analyses compared with some of the other samples, we consider the age of this dike as 48–47 Ma.

[29] Zircons from the isolated leucogranite boudins shown in Figure 4e (Sample 10PC30) yield 18 ages between 51.4 ± 2.0 and 42.8 ± 1.6 Ma (ICPMS), with only one Precambrian grain. Fourteen of these are between 44.0 ± 2.0 and 47.6 ± 1.9 Ma, yielding a weighted mean of 45.7 ± 0.8 Ma (Figure 7b).

[30] A steeply dipping meter-thick dike (Figure 4c) that cuts the dominant fabric with the WNW-trending lineation was dated on the SHRIMP. Zircons from this sample (10PC33) yielded almost entirely Eocene ages with 22 grains giving a weighted mean age of 45.9 ± 0.3 Ma (Figure 7c).

[31] Together, these ages indicate that pervasive strain accumulated in the lower part of the Middle plate at or after 48–47 Ma, and that strain ceased, at least locally, by ~46 Ma. The boudinaged sample 10PC30 (Figures 4e and 7b) comes from higher in the section than the undeformed dike (Figures 4b and 7c). The uncertainties of this ICPMS age overlap with both the deformed and undeformed dikes (Figure 4). Therefore, it is not clear if strain continued after ~46 Ma in this higher part of the section. However, we note that undeformed crosscutting dike segments are present here, but overall dikes decrease in abundance upsection making direct comparison with deeper levels difficult. The data do not allow determination as to whether strain also occurred prior to 48–47 Ma.

5.2. Lower Plate

[32] Sample 09PC55 comes from a leucogranite boudin (Figure 5f) in the Wildhorse Lakes area. Most grains show inheritance from a Neoarchean source, while five grains yield SHRIMP ages between 54.8 ± 0.8 and 60.8 ± 0.8 Ma, with a single spot at 47.1 ± 0.8 Ma (Table 1a). From these data, it is difficult to assign a crystallization age to this leucogranite, other than Paleocene to Early Eocene.

[33] Sample 09PC56 also comes from the Wildhorse Lakes area, but is structurally below sample 09PC55. It consists of strongly foliated, leucocratic augen gneiss that intruded meta-psammitic gneiss (Figure 5e). Because of inheritance and the interlayering of the protolith and leucogranite, most grains yielded Precambrian ages. However, five Eocene grains were dated by ICPMS and have a weighted mean of 48.9 ± 0.6 Ma (Figure 8a and Table 1b). Two additional grains were dated on the SHRIMP, giving ages of 48.3 and 50.8 Ma (Table 1a).

[34] Two other samples from different areas of the Lower plate have also been dated. These samples do not date the top-WNW strain, but bear on the general age of strain and high-grade metamorphism. Sample 09PC15, from the steep

Table 2. Summary Table for U-Pb Samples

Sample	Latitude	Longitude	Type of Analysis	Weighted Mean $^{238}U/^{206}Pb$ Age (Ma)	Figure	Structural Relations
			Middle Plate			
09PC61	43° 46.662′	114° 10.834	SHRIMP	47.1 ± 0.7	4d, 7a	Isoclinally folded, lineated felsic dike
10PC30	43° 45.663′	114° 10.501′	ICPMS	45.7 ± 0.8	4e, 7b	Boudins of leucogranite dikes
10PC33	43° 45.625′	114° 10.317′	SHRIMP	45.9 ± 0.3	4b, 7c	Crosscutting, post-kinematic felsic dike
			Lower Plate			
05PCRM01	43° 45.183′	114° 6.541′	ICPMS	52.3 ± 1.8	8d, 8e	Layered migmatite
09PC15	43° 47.933′	114° 05.433′	SHRIMP	49.4 ± 0.5	8b, 8c	Isoclinally folded leucogranite
09PC55	43° 45.586′	114° 06.923′	SHRIMP	Eocene	5f	Leocogranite boudin
09PC56	43° 45.622′	114° 06.874′	ICPMS	48.9 ± 1.2	5e, 8a	Leucogranite layer with solid-state foliation
			Pioneer Intrusive Suite			
05PC28	43° 45.247′	114° 07.216′	SHRIMP	48.6 ± 0.4	9a	Magmatically foliated granodiorite
09PC28	43° 47.342′	114° 09.678′	SHRIMP	49.4 ± 0.4	9b	Magmatically foliated biotite granite

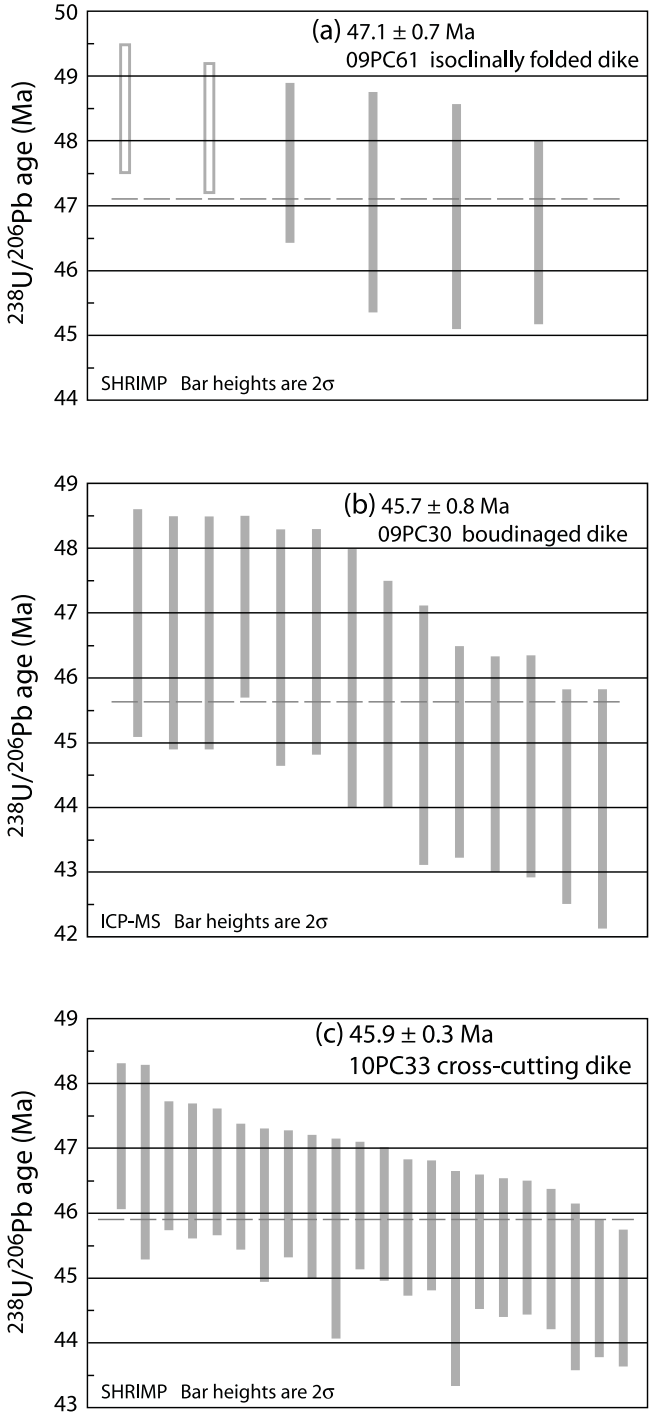

Figure 7. U-Pb age data from Middle plate. Complete data are shown in Tables 1a and 1b and additional plots are provided in the auxiliary material. Type of analysis shown in bottom left corner of each plot. (a) Weighted-mean plot of Eocene grains from folded leucogranite dike (sample 09PC61) shown in Figure 4a. Only solid bars are used in age calculation. See text for discussion. (b) Weighted-mean plot of Eocene grains from leucogranite boudins (sample 10PC30) shown in Figure 4e. (c) Weighted-mean plot of Eocene grains from planar, crosscutting dike (sample 10PC33) shown in Figure 4b.

east flank of the Wildhorse dome, is an isoclinally folded leucogranite dike (Figure 8b). The high-temperature axial-planar fabric is the dominant strain fabric in this region. This sample yielded ten grains between 48.6 and 50.8 Ma with a weighted mean of 49.4 ± 0.5 Ma (Figure 8c), as well as several other Early Eocene grains. Sample 05PCRM01 is a layered migmatite from the south-central part of the Wildhorse dome (Figure 8d). This sample dated via ICPMS contains abundant Paleoproterozoic grains and eight Early Eocene grains, which yield a weighted mean of 52.3 ± 1.8 Ma (Figure 8e).

[35] Together, these data show that in the Lower plate, high-grade metamorphism and associated structural fabrics are Eocene in age. Furthermore, on the west flank of the dome this strain has a component of top-west shear that occurred at high temperatures at or after ~50–49 Ma.

5.3. Pioneer Intrusive Suite

[36] Sample 05PC28 comes from a magmatically foliated granodiorite on the southwest flank of the Wildhorse dome. Rocks in this area are petrographically similar to the granodiorite in the Kane Creek area and are considered the southern continuation of that magmatic sheet. Fifteen grains analyzed by SHRIMP, all within 2σ error, yield a weighted-mean age of 48.6 ± 0.4 Ma (Figure 9a).

[37] Sample 09PC28 comes from a magmatically foliated porphyritic biotite granite sill in the Kane Lake area. SHRIMP ages from this sample are more scattered than 05PC28 and display three peaks between ~49 and 53 Ma (Figure 9b). The weighted mean age of ten grains defining the youngest group is 49.4 ± 0.4 Ma and represents the best estimate of the age of crystallization. The older zircons most likely crystallized in earlier Eocene magmas and were inherited.

[38] Three other samples from the eastern PIS were also dated, yielding robust ages between 47 and 49 Ma. These data indicate that most of the volume of the PIS was emplaced in less than 3 m.y., between 50 and 47 Ma.

6. Discussion

6.1. Age of Metamorphism and High-Temperature Strain in the Lower Plate

[39] The U-Pb data from the Lower plate indicate that widespread felsic injections, local melting, and high-grade metamorphism are Eocene in age. In addition to data presented here, numerous Early Eocene grains and rims were found by *Durk* [2007], *Cameron* [2010], and Link and Fanning (unpublished data, 2006–2010) in their studies of the protolith ages of the Lower plate. These new data contrast with the interpretations of *Dover* [1983] and *Silverberg* [1990], who suggested that high-grade metamorphism and associated strain fabrics in the Wildhorse gneisses of the Lower plate occurred in the Late Cretaceous. Silverberg's interpretation was based on an $^{40}Ar/^{39}Ar$ hornblende spectrum with ~79 Ma ages for the high-temperature steps. Widespread zircon growth in metamorphic rocks and in situ partial melting indicate that temperatures well above the argon closure temperature of hornblende were widespread through the Lower plate in the Eocene. Thus, the hornblende may contain excess argon or retained its gas from an earlier

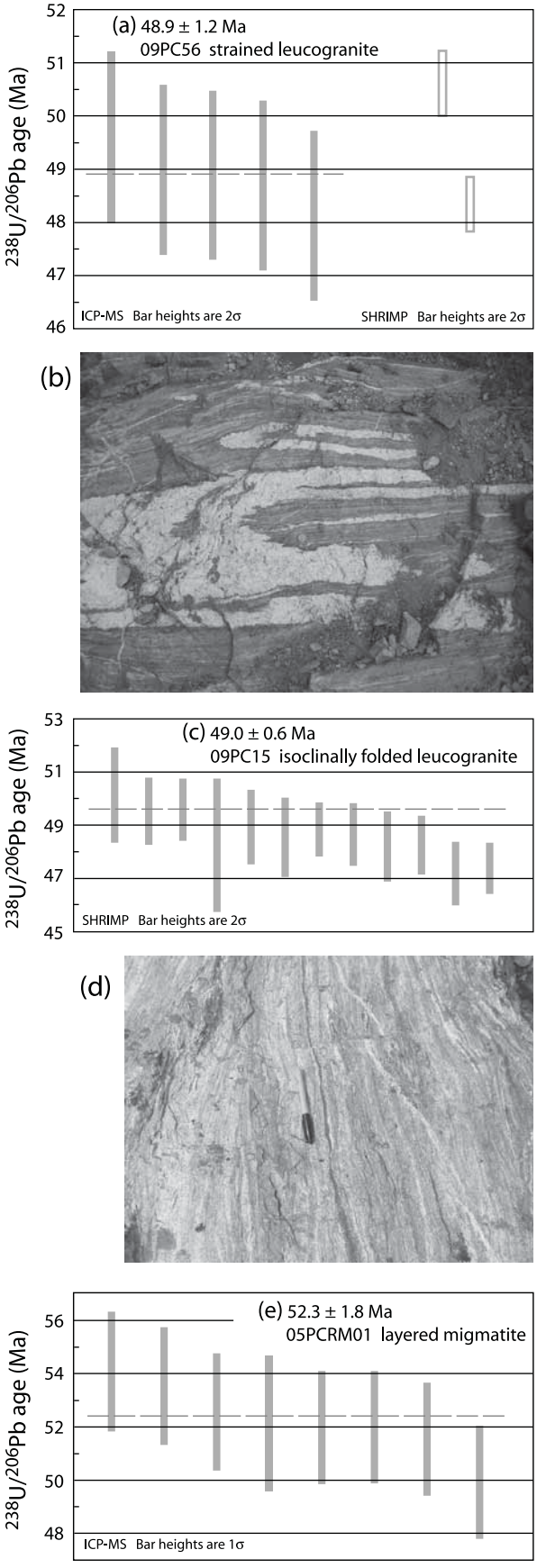

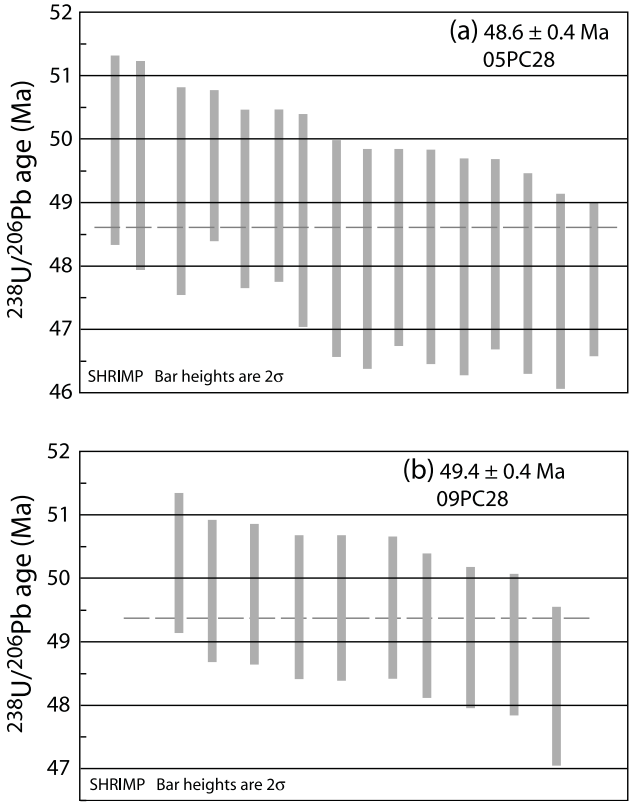

Figure 9. U-Pb data from Pioneer intrusive suite. Complete data are shown in Tables 1a and 1b and additional plots are provided in the auxiliary material. Type of analysis shown in bottom left corner of each plot. (a) Weighted-mean plot of Eocene grains from magmatically foliated granodiorite on western flank of Wildhorse dome (sample 05PC28). (b) Weighted-mean plot of Eocene grains from magmatically foliated porphyritic biotite granite sill in Kane Creek area (sample 09PC28).

Cretaceous event, which we consider unlikely. Our data do not preclude a Cretaceous metamorphism, but indicate that any earlier events have been severely overprinted in the Eocene. Given the relationship between the high-temperature

Figure 8. U-Pb age data and photos from Lower plate. Complete data are shown in Tables 1a and 1b and additional plots are provided in the auxiliary material. Type of analysis shown in bottom left corner of each plot. (a) Weighted-mean plot of Eocene grains from deformed leucogranite shown in Figure 5e (sample 19PC56). Solid bars dated on SHRIMP and open bars dated on ICPMS. (b) Photo of isoclinal fold of leucogranite in Lower plate from subvertical east flank of Wildhorse dome. Age information in Figure 8c. See Figure 2 for location. (c) Weighted-mean plot of Eocene grains from folded leucogranite shown in Figure 8b (sample 09PC15). (d) Photo of layered migmatite in Lower plate. Age information shown in Figure 8e. See Figure 2 for location. (e) Weighted-mean plot of Eocene grains from migmatite shown in Figure 8d (sample 05PCRM01).

strain and Eocene melt, it is clear that most, if not all of the strain preserved in the Lower plate formed during Eocene extension.

6.2. Extensional History of the PCC

[40] The AMS and magmatic fabrics in the northwestern PIS sheet along with the U-Pb data indicate that WNW-directed extension was ongoing by 50–49 Ma, and that ductile deformation continued after ~48–47 Ma, but ceased, at least locally, by ~46 Ma. Although 50 Ma represents a minimum age for the onset of ductile extensional strain, the large strains in the Lower plate and the minimal solid-state fabrics in the PIS may indicate that some strain accumulated prior to 50 Ma.

[41] Ductile strain during this period appears to have been concentrated along the Middle-Lower plate boundary where subhorizontal magmatic sheets of the PIS were injected, suggesting that strain may have been localized by the melt and heat during intrusion. This strain produced homogeneous magmatic/magnetic foliations and lineations in the PIS, as well as extensive foliations, WNW-trending lineations, and isoclinal folds and boudins of Eocene granitic injections within the enclosing metamorphic rocks. This phase of ductile extension overlapped with extensive dike injection and local melting within the lower plate. Together, these observations show that in the northwest part of the core complex, strain occurred in all three units across the Middle-Lower plate boundary and was kinematically coupled through the structural section. The lack of suitable metamorphic mineral assemblages precludes the reconstruction of the P-T history of the Lower plate and quantification of the amount of extensional exhumation beneath this shear zone during this high-temperature event.

[42] The map-scale folds in the North Fork Hyndman Creek area (Figure 3), as well as smaller scale folds to the south, commonly have NE-vergent asymmetries. The parallelism between the fold hinges and the Eocene D_{2E} stretching lineations, as well as the spatial association between the folds and lineations suggests that the folds may also be Eocene. This interpretation is further suggested by the observation of the involvement of a dike with a NE-vergent mesoscopic fold in the southern part of the area. Such folds may be the result of a component of NE-directed horizontal shortening during extension [*Vogl et al.*, 2011]. This shortening may have produced the larger scale elongate Wildhorse dome, which also has a NE-vergent asymmetry.

[43] Following top-WNW ductile strain along the Middle/Lower plate boundary, shear strain appears to have been partitioned into the Wildhorse detachment after ~46 Ma when late crosscutting dikes were emplaced. Whether 46 Ma represents the beginning of a hiatus in extension or repartitioning of extensional strain is not clear. Deactivation of the Middle/Lower plate boundary shear zone occurred while the temperatures remained above $^{40}Ar/^{39}Ar$ hornblende closure temperatures (45–44 Ma ages of *Silverberg* [1990]). Repartitioning of the strain is likely the result of cooling, re-orientation of the shear-zone layering during doming, and changing rheologic distribution following crystallization of the large stock-like body of the eastern PIS. Details of the timing, cause, and kinematics of dome formation are still under investigation, but it appears that doming occurred at high temperatures and probably prior to emplacement of the 48–47 Ma (unpublished) eastern PIS body, which is limited to the east side of the Wildhorse dome, compared to the western granodiorite that wraps around the dome. In the northwest corner of the footwall, the high-temperature fabrics grade upsection into lower temperature mylonites, suggesting that where the Wildhorse detachment occurs in close proximity to the Middle/Lower plate boundary, D_{2E} strain may be the composite between these two shear zones. Farther south, strain in the Middle plate appears to decrease upsection (Figure 2) and there is little or no ductile fabric associated with the Wildhorse detachment.

[44] While field relationships combined with U-Pb ages clearly define the age of early high-temperature extensional strain, the subsequent extensional history can be inferred from the cooling history. The thermal history shown in Figure 10 was constructed by combining new U-Pb and (U-Th)/He ages with the $^{40}Ar/^{39}Ar$ data of *Silverberg* [1990]. The early cooling from high temperatures is likely related to a combination of extensional denudation and conductive cooling following emplacement of the mid-crustal intrusions. Cooling continued through the Middle and Late Eocene with average rates of 25°–30°C. The presence of Challis volcanics preserved around the perimeter of the PCC indicates that less than ~1–2 km of erosion has occurred in the region since ~45 Ma and therefore exhumation was localized in the PCC rather than being part of a regional erosional denudation event. Thus, *Silverberg* [1990] interpreted 38–33 Ma WNW-directed motion on the Wildhorse detachment to produce cooling between the mica and K-feldspar ages.

[45] It is not clear whether WNW-directed extension occurred continuously between 50 and 33 Ma or whether the 38–33 Ma extension represents a distinct episode that was kinematically similar to the 50–46 Ma strain. Both brittle and ductile features along the detachment indicate WNW-directed motion [*Wust*, 1986; *O'Neill and Pavlis*, 1988], suggesting protracted unidirectional motion. Cooling rates slowed dramatically after ~32 Ma until a regional ~11–9 Ma exhumation event, which is recorded by (U-Th)/He apatite dating [*Vogl et al.*, 2010; *Carmenate et al.*, 2011].

6.3. Relationship With Volcanism and Extension in the Upper Plate

[46] NW-directed extensional strain, magmatism, and partial melting in the footwall of the PCC was also synchronous with lava flows, emplacement of numerous rhyolite/dacite domes, and explosive volcanism in regions immediately adjacent to the PCC. These volcanic rocks of the southeast Challis volcanic field have yielded $^{40}Ar/^{39}Ar$ ages between 50 and 47 Ma [*Snider*, 1995; *Sanford*, 2005].

[47] WNW-directed extension along the Middle/Lower plate boundary in the PCC at 50 to 46 Ma is kinematically compatible with numerous syn-Challis features immediately adjacent to the PCC, as well as regionally. NE-trending, Challis-age dikes and dike swarms can be found throughout central Idaho, including in the upper plate immediately adjacent to the PCC [*Dover*, 1981; *Bennett*, 1986; *Janecke*, 1992; *Snider*, 1995; *Worl and Johnson*, 1995; *Skipp et al.*, 2009]. The NE-striking Trans-Challis extensional fault system was active during Challis volcanism and plutonism [*Bennett*, 1986; *Janecke et al.*, 1997]. NW-directed shearing

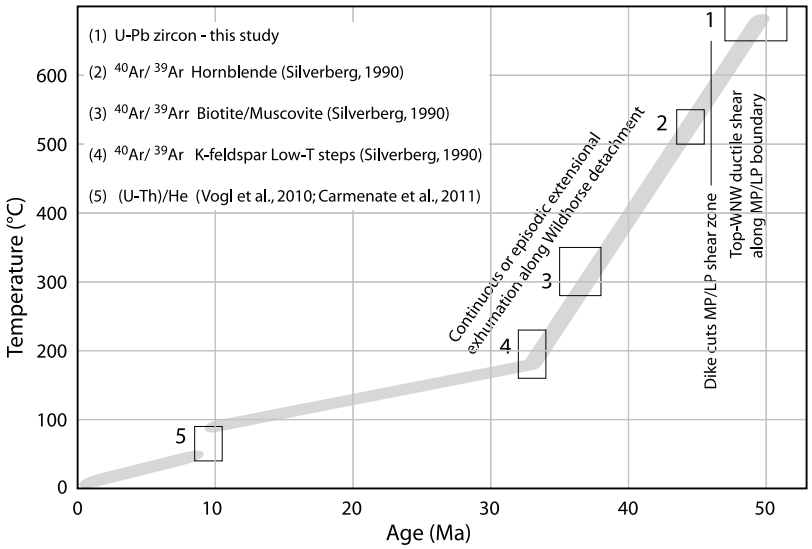

Figure 10. Thermal history of PCC. $^{40}Ar/^{39}Ar$ data are from *Silverberg* [1990]. Hornblende ages represent only the plateau or near-plateau ages from *Silverberg* [1990]. K-feldspar data refer to low-temperature steps only. (U-Th)/He data from *Vogl et al.* [2010] and *Carmenate et al.* [2011].

on shallow SW-dipping strike-slip faults in the upper plate immediately to the southwest of the PCC [*Rodgers et al.*, 1995; *Huerta and Rodgers*, 1996; *Diedesch*, 2011] were also likely active during the earliest stages of shearing along the Middle/Lower plate boundary. Numerous NE-trending normal faults mapped by *Janecke* [1992] east of the PCC in the Lost River and Lemhi Ranges were also active during early Challis volcanism.

[48] The Middle/Lower plate boundary may be a mid-crustal, ductile shear zone along which west-northwest translation of the upper plate occurred. However, the geometric and kinematic linkage between the mid-crustal shear zone and upper plate structures is not clear and, given the fact that significant strain may have accumulated prior to extensive 48–47 Ma ash flows and dacite/rhyolite domes [*Snider*, 1995], the earliest formed upper plate structures may be largely obscured. If this shear zone is the mid-crustal segment of a detachment fault, a potential breakaway is an unnamed fault located 30–35 km southeast of the PCC shown on the map of *Skipp et al.* [2009].

[49] The total amount of horizontal extension associated with development of the PCC is difficult to document precisely, but is likely between about 12 and 32 km. Combining fault dip estimates of 30°–45° with contact aureole depth estimates (12–15 km) yields 12–26 km of horizontal displacement. Estimates of ~15–16 km and ~30–32 km are obtained by correlation of the eastern PIS with the Summit Creek stock (Figure 2) and North Fork Lake quartz porphyry dike complex, respectively, within the upper plate to the west-northwest [e.g., *Wust*, 1986; *Silverberg*, 1990]. We note that these estimates refer to displacement after emplacement of PIS magmas and that additional extension may have occurred along the Middle/Lower plate boundary prior to intrusion.

6.4. Comparison With Previous Interpretations

[50] Our results indicate that the penetrative fabrics in the Lower plate and lower section of the Middle plate of the PCC record Eocene extensional strain and are not relicts of Cretaceous shortening and associated metamorphism as suggested by *O'Neill and Pavlis* [1988] and *Silverberg* [1990]. Furthermore, top-WNW extensional strain was previously interpreted to be localized along the Wildhorse detachment and in discrete undated small-scale shear zones in the footwall [*Wust*, 1986; *O'Neill and Pavlis*, 1988; *Silverberg*, 1990], but appears to be far more widespread in the footwall than previously recognized. This discrepancy may be due to the fact that previous descriptions of detachment-related ductile strain appear to focus on mylonitic fabrics associated with obvious grain-size reduction. Our new observations, however, are largely from rocks with higher temperature fabrics, but are kinematically similar to both the lower-T mylonites and the brittle features.

[51] Last, top-WNW strain was pervasive along the Middle/Lower plate boundary during intrusion of the PIS, an observation that conflicts with *Silverberg*'s [1990] interpretation of SSW-side-down extensional shearing localized at the Middle/Lower plate contact (his Hyndman shear zone). Overall, top-WNW strain in the footwall is more kinematically compatible with synchronous upper plate structures and therefore does not require mid-crustal levels that were stretching orthogonally to upper crustal structures. We have observed S- to SSW-plunging sillimanite lineations in a few areas, but orientations tend to be highly variable over short distances. Furthermore, lineation orientations in the Lower plate vary around different parts of the dome, but these are likely related to strains during the doming process (which may have overlapped with WNW shearing) or may predate emplacement of the PIS.

7. Regional Variations in the Rates of Extension and Core Complex Development

[52] WNW-ESE extension in the PCC at ≥50 to ~46 Ma documented here was synchronous with the major period of core-complex development from Idaho into British

Columbia. For example, extension in the Bitterroot and Anaconda core complexes to the north began at ~53 Ma [*Foster and Fanning*, 1997; *Foster et al.*, 2001, 2007, 2010], ≤1–2 my after the end of thrusting in the foreland [*Constenius*, 1996]. Although the core complexes of Canada may have complicated exhumation histories, it seems clear that there was a major extensional event that occurred throughout the Early Eocene and began around 55–54 Ma [e.g., *Tempelman-Kluit and Parkinson*, 1986; *Parrish*, 1995; *Johnson and Brown*, 1996; *Hinchey et al.*, 2006]. Despite the synchroneity of extension in the region, comparison of thermal and metamorphic histories suggests that the rates of core complex exhumation during the Early Eocene decreased southward into south-central Idaho.

[53] Available data do not allow a precise quantification of extension rates throughout the different regions, however, first-order differences can be estimated by comparison of the amount of crust cooled through a specific temperature during a given time interval within each core complex (i.e., an estimate of the amount of extensional exhumation during a given time interval). In Figure 11 we show the variations in published U-Pb and $^{40}Ar/^{39}Ar$ ages associated with each core complex. In Figure 12, we show the present distribution of footwall metamorphic rocks with mica $^{40}Ar/^{39}Ar$ ages of ≥47 Ma (47 Ma represents the youngest widespread cooling age in the northern core complexes), which provides an estimate of the amount of presently exposed metamorphic footwall exhumed through the middle crust by the end of the Early Eocene. It is important to note that most of the areas shown in blue in Figure 12 were at temperatures in excess of 550–650°C during the Paleocene to Early Eocene as indicated by zircon and/or monazite U-Pb ages (Figure 11). Only the Kettle [*Laberge and Pattison*, 2007] and Anaconda core complexes [*Foster et al.*, 2010] show evidence for Late Cretaceous cooling. This distinction is important because areas with Early Eocene and Paleocene ages require larger amounts of Early Eocene cooling/exhumation, whereas Cretaceous U-Pb ages leave open the possibility of partial exhumation during the Late Cretaceous.

[54] Figures 11 and 12 show that in the core complexes north of the Lewis and Clark line, nearly all of the exposed footwalls cooled through argon mica closure (~300°C) by 47 Ma. Combined with metamorphic data that indicate depths of >25 km immediately prior to Early Eocene extension in several areas [e.g., *Foster et al.*, 2004; *Hinchey et al.*, 2006], the cooling data show that extensive areas of deep-seated metamorphic rocks were exhumed through the middle crust by 47 Ma. South of the Lewis and Clark line, only the western half of the currently exposed Bitterroot and Anaconda complexes cooled below ~300° by 47 Ma. Farther south, none of the presently exposed footwall of the PCC cooled through mica closure until at least 38 Ma.

[55] The difference in amount of extensional exhumation between ~55–53 Ma and 47 Ma, can be illustrated through comparison of data across transects A and B in Figure 12.

[56] Combining the width of the core complexes with pressure/depth estimates immediately prior to 55–53 Ma extension (and assuming a 10 km depth for the 300°C isotherm) allows rough estimates of cross-sectional areas exhumed through the middle crust during the Early Eocene.

[57] Along transect A, metamorphic pressures of ≥7–8 kb have been estimated at 55–53 Ma for the Monashee complex [*Norlander et al.*, 2002; *Foster et al.*, 2004; *Hinchey et al.*, 2006]. Thus, combining the 25 km width and a depth estimate of 25 km, suggests that >~375 km^2 were exhumed through ~10 km depth (300°C isotherm) by 47 Ma. The Selkirk allochthon spans an additional ~50 km along transect A (Figure 12) and also has mica $^{40}Ar/^{39}Ar$ ages of 50–47 Ma (Figure 12). U-Pb zircon and monazite ages are as young as 55 Ma, indicating that it was at high temperatures into the Early Eocene. Thus, there was very rapid cooling in at least parts of the Selkirk allochthon between 55 and 47 Ma. However, several studies have proposed channel flow within the northern Shuswap complex [e.g., *Johnston et al.*, 2000; *Glombick et al.*, 2006; *Kuiper et al.*, 2006], suggesting a potentially complex exhumation history involving multiple mechanisms. Most recently, *Gervais and Brown* [2011] have argued that this area was partially exhumed into the upper middle crust via synconvergent channel flow by 55 Ma. If this model is correct, then large amounts of exhumation may not have occurred in the Selkirk allochthon during the extensional phase beginning at 55–53 Ma. Channel-flow exhumation notwithstanding, it seems likely that some exhumation occurred through motion on the bounding detachments, and even a couple kilometers could increase the extensional exhumation estimate along this transect by over 100 km^2. Although farther south, semi-quantitative analysis is more difficult, the exposed widths of footwalls yielding $^{40}Ar/^{39}Ar$ mica ages ≥47 Ma between the Monashee complex and the Lewis and Clark line suggests large amounts of extensional exhumation in these areas also. Furthermore, metamorphic data also suggest much more exhumation occurred between 55 and 47 Ma in some of these areas (particularly the Valhalla [e.g., *Spear and Parrish*, 1996]) and western part of the Okanagan complex [*Hansen and Goodge*, 1988; *Kruckenberg and Whitney*, 2011] compared with the core complexes in Idaho.

[58] Of the areas along transect B (Figure 12) with mica $^{40}Ar/^{39}Ar$ ages of ≥47 Ma prior to 53 Ma extension, the western Bitterroot core complex was at depths of only 5–15 km [*Foster et al.*, 2001] and the western Anaconda core complex was immediately below the mica argon partial retention zone [*Foster et al.*, 2010]. Taking the 20 km width of the western Bitterroot core complex with an average depth of 15 km, yields only ~100 km^2 of exhumation through a depth of 10 km by 47 Ma. Given the preservation of a biotite argon partial retention zone in the western Anaconda core complex [*Foster et al.*, 2010], exhumation by 47 Ma in this area was minimal.

[59] A full quantitative analysis of exhumation would require knowing the exact depth distribution of footwall rocks immediately prior to the onset of extension, the 3-D geometry of the isochrons, and cooling ages of the unexposed and eroded portions of the footwalls. Nonetheless, despite the simplifications of this analysis, a strong case can be made for distinct north-south differences in extensional exhumation rates. Specifically, the data show that significantly more (perhaps 3–4 times) footwall exhumation occurred in the north than the south in the period between 55 and 53 Ma and 47 Ma, suggesting higher rates of extension in the north. This conclusion is reinforced when normal-fault bounded regions of metamorphic rocks with mica ages >47 Ma, such as the North Cascades crystalline core, [e.g., *Paterson et al.*, 2004], Coast Mountains of British

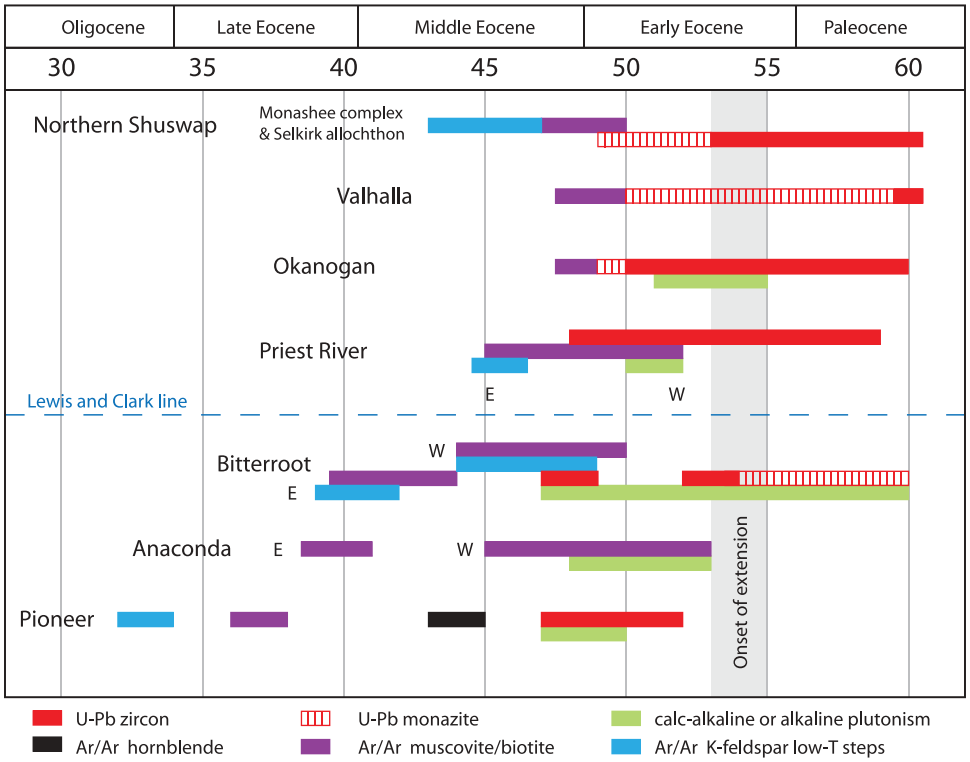

Figure 11. Comparison of U-Pb and $^{40}Ar/^{39}Ar$ data from Cordilleran core complexes. Note that in many cases monazite ages overlap with zircon ages, in which case we only show the monazite ages that do not overlap. Similarly, only youngest mica ages are shown where older ages overlap with ages from higher temperature systems. Data from Northern Shuswap [*Parrish et al.*, 1988; *Carr*, 1992; *Parrish*, 1995; *Crowley*, 1999; *Vanderhaeghe et al.*, 1999; *Crowley et al.*, 2001; *Foster et al.*, 2004; *Teyssier et al.*, 2005; *Hinchey et al.*, 2006; *Gervais et al.*, 2010], Valhalla [*Carr and Simony*, 2006; *Spear and Parrish*, 1996; *Gordon et al.*, 2008], Okanagan [*Kruckenberg et al.*, 2008; *Brown et al.*, 2010], Priest River [*Harms and Price*, 1992; *Doughty and Price*, 1999; *Doughty and Chamberlain*, 2004], Bitterroot [*House et al.*, 1997; *Foster et al.*, 2001, 2007, 2010; *Baldwin et al.*, 2011], and Pioneer [*Silverberg*, 1990; this study].

Columbia [e.g., *Andronicos et al.*, 2003], and Kootenay arc [e.g., *Archibald et al.*, 1984] are considered along with the other core complexes. Thus, the Lewis and Clark line may not only represent a transfer zone that offsets the locus of large-magnitude extension, it may also accommodate a decrease in extensional rates. Regardless of the exact nature of the southward decrease, it is clear that the PCC region represents a significant reduction in the amount of Early Eocene extensional exhumation.

[60] This analysis assumes that all cooling is related to exhumation. This is a reasonable assumption for the northern core complexes where the footwalls were cooling from regional high-grade conditions, and for the Idaho and Montana core complexes where cooling is up to 10 m.y. younger than the age of the plutons, and progresses in the direction of detachment slip, as in the case of the Bitterroot and Anaconda complexes. Furthermore, the 10–12 m.y. difference between emplacement of the ~500 m pluton sheet and cooling below ~300°C for the PCC is enough time for cooling to ambient conditions, suggesting that the $^{40}Ar/^{39}Ar$ mica ages are exhumation-related.

[61] Within Idaho, the southward decrease in the rate of exhumation continued through the Middle Eocene. Metamorphic and migmatite U-Pb zircon ages as young as 53, 50, and 48 Ma have been reported for the northeastern Bitterroot core complex [*House et al.*, 1997; *Foster et al.*, 2001; *Baldwin et al.*, 2011], as well as mica $^{40}Ar/^{39}Ar$ ages of 42–40 Ma, and 42–39 Ma ages for low-T $^{40}Ar/^{39}Ar$ K-feldspar steps [*Foster et al.*, 2001]. Although the PCC has similar migmatite ages, mica ages are 38–36 Ma and K-feldspar low-T steps are 33–32 Ma [*Silverberg*, 1990], indicating that exhumation-related cooling during the Middle to Late Eocene may have been significantly faster in the eastern Bitterroot core complex than in the PCC.

[62] In the core complex regions south of the Snake River plain, a small number of Eocene $^{40}Ar/^{39}Ar$ cooling ages have been reported from the Wood Hills, ARG and REH core complexes (see Figure 1) [*Thorman and Snee*, 1988; *McGrew and Snee*, 1994; *Wells et al.*, 2000]. In none of these areas, however, is an Early Eocene cooling event defined by multiple thermochronometers. In fact, most other lower temperature thermochronometers constrain the amount of Early to Middle Eocene cooling to be relatively minor. Furthermore the Wood Hills and REH core complex expose rocks with Late Cretaceous (≥75 Ma) ages for peak metamorphism at structural levels of the sample locations. Overall, for these areas south of the SRP, although there is scattered evidence for local cooling and minor tilting

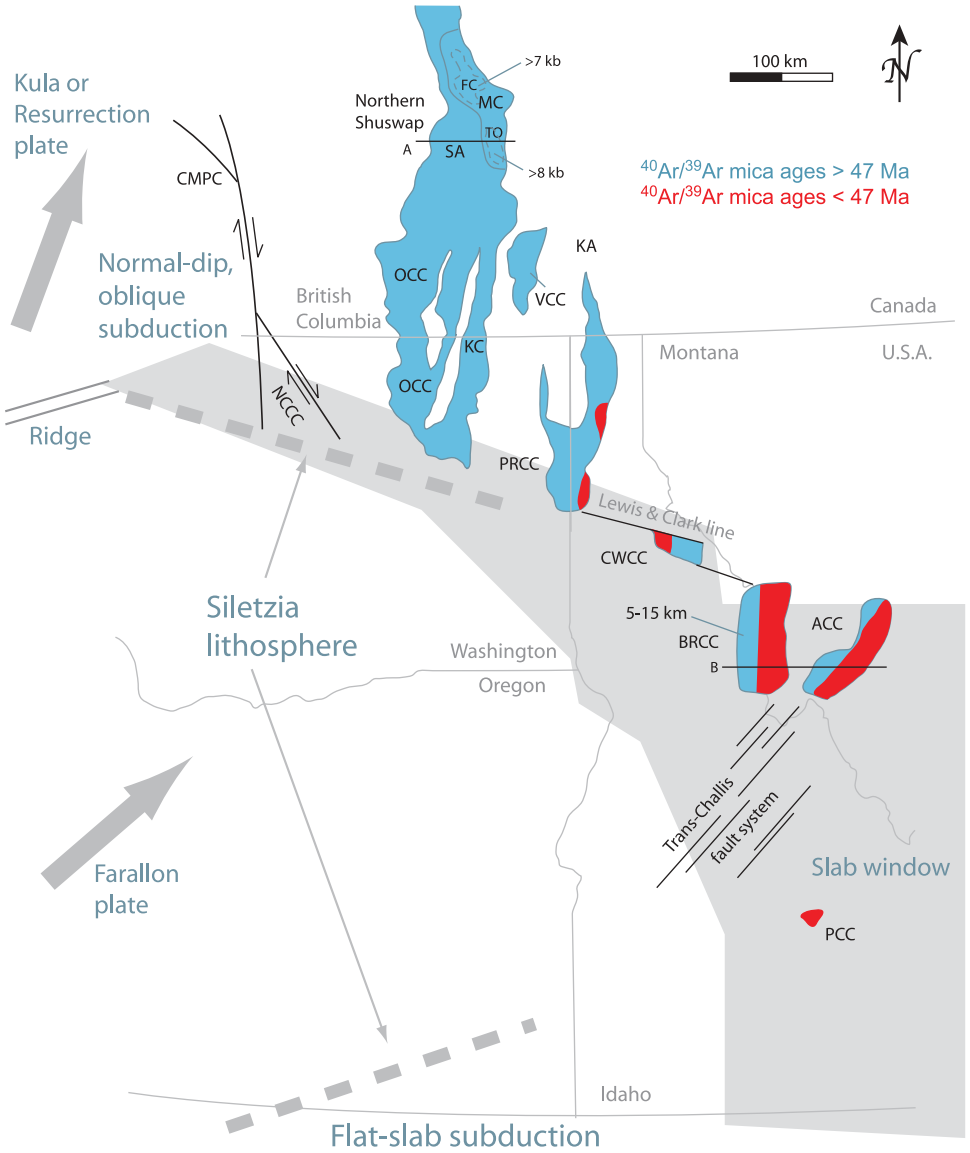

Figure 12. Map showing Early Eocene tectonic setting and $^{40}Ar/^{39}Ar$ mica ages from the northern Cordilleran core complexes. Based on data from Figure 11. Exhumation estimates along transects A and B are discussed in text. Estimates for metamorphic pressures immediately prior to 55–53 Ma extension are shown for Frenchman Cap dome [*Foster et al.*, 2004] and Thor-Odin dome [*Hinchey et al.*, 2006]. Depth estimates for the western Bitterroot core complex [*Foster et al.*, 2001] for the same time are also shown. Gray shaded area represents region proposed to be underlain by a slab window at ~50 Ma [*Breitsprecher et al.*, 2003]. Siletzia lithosphere from *Gao et al.* [2011]. Abbreviations: ACC, Anaconda core complex; BCC, Bitterroot core complex; CMPC, Coast Plutonic complex; FC, Frenchman cap dome; KA, Kootenay arc; KC, Kettle complex; MC, Monashee complex; NCCC, North Cascades crystalline core; OCC, Okanogan core complex; PRCC, Priest River core complex; SA, Selkirk allochthon (lower); TO, Thor-Odin dome; VCC, Valhalla core complex.

[*Potter et al.*, 1995; *Dubiel et al.*, 1996; *Henry*, 2008] during the Early and/or Middle Eocene, there are no data that conclusively document a cooling/exhumation event or basin formation attributable to large-magnitude extension. Thus, given the available data, we consider Early Eocene to be minimal south of the Snake River plain.

[63] The discussion above suggests three core-complex domains: a northern domain with high rates of extensional exhumation north of the Lewis and Clark line, a central domain in central Idaho with distinctly slower rates, and a southern domain south of the Snake River plain where regional Early Eocene extension was minimal. Thus, the PCC and its relatively low rates of extension may represent the southern end of the Early Eocene extensional domains. We note that core-complex exhumation rates may not directly correlate with region-wide extension rates, however,

because of younger cover rocks, it is difficult to construct an orogen-scale cross-section in the Oregon-Idaho region to more completely address regional extension.

8. Geodynamics of Extension

[64] The core-complex domains discussed above have implications for the geodynamic factors controlling extension. Many factors likely play a role in the timing, rates, spatial distribution, and character of extension. The extensional domains lie above segments of a subduction margin that had different characteristics along strike in the Early Eocene (Figure 12), suggesting a link between extensional rates and subduction geometry/kinematics. The northern domain was above a subduction zone with a normal dip, whereas south of the Snake River plain, shallow subduction persisted at this time [e.g., *Humphreys*, 2009; *Foster et al.*, 2010], likely inhibiting extension. In the intervening area, the lower rates of extension in the central Idaho region could result from transitional slab dips or may have been controlled by slab removal following the accretion of Siletzia along the Oregon coast [*Humphreys*, 2008, 2009; *Schmandt and Humphreys*, 2011; *Gao et al.*, 2011]. Alternatively, higher rates of core-complex development in the northern domain may have been controlled by more oblique subduction of the Kula or Resurrection plate (Figure 12) [e.g., *Engebretson et al.*, 1985; *Thorkelson and Taylor*, 1989; *Haeussler et al.*, 2003; *Madsen et al.*, 2006] and/or related strike-slip faulting [*Ewing*, 1980; *Price and Carmichael*, 1986; *Umhoefer and Schiarizza*, 1996] that is well documented to the west and north of these core complexes.

[65] Early Eocene magmatism and extension have also been attributed to a slab window from central Idaho to southern British Columbia that resulted from subduction of the Farallon/Kula or Farallon/Resurrection ridge [*Breitsprecher et al.*, 2003; *Madsen et al.*, 2006]. Such a slab window could have played a role in Challis magmatism. South-central Idaho, however, was the site some of the most voluminous Eocene volcanism, as well as the largest proposed slab-free area (Figure 12), and therefore might be expected to have had the greatest effects of thermal weakening and uplift from the asthenospheric upwelling in the window, yielding high rates of extension. The comparatively low rates of extension in the central Idaho core complexes, however, suggest that a slab window is unlikely to be a primary factor controlling extension rates in Idaho.

[66] Moreover, the different extensional rates may instead be related to differences in the size and thermal state of the orogenic wedge [e.g., *Beaumont et al.*, 2006]. In particular, the Canadian core complexes may have been a part of a wider, hotter, and therefore weaker orogen allowing faster rates of extensional collapse compared with central Idaho.

9. Conclusions

[67] Our new data and observations provide a new view of extension within the Pioneer core complex that is more compatible with the timing and directions of extension in other core complexes of the region. We have shown that the crustal section in the northwestern footwall of the PCC records top-WNW extensional strain from ≥50 Ma to 46 Ma. This strain affected all of the Middle and Lower plates in this area, as well as the intervening synkinematic granodiorite sheet. Farther south, however, Eocene strain in the Middle plate is confined to the deeper parts of the section. The kinematics determined from our study conflict with earlier models that had fewer geochronologic constraints. Field observations and U-Pb data from other parts of the Lower plate indicate that high-grade metamorphism and associated high strains are Eocene in age rather than Cretaceous as previously assumed.

[68] The timing of footwall strain coincides with the development of all core complexes to the north, into British Columbia. However, it appears that extension in the PCC has produced distinctly slower exhumation rates than to the north and is part of a southward decrease in the rates of footwall exhumation. The spatial variations in exhumation rates coincide with spatial differences in the both the subducting plate characteristics and possibly the nature and strength of the orogenic wedge.

[69] Although we have clearly documented top-WNW extensional strain from ≥50 Ma to 46 Ma, other structural observations from around the Wildhorse dome (Figure 2) show that 3-D strain patterns at deeper levels are more complex and are also the result of Early Eocene deformation. This full 3-D strain history recorded by these deeper lineations and by the Wildhorse dome remains the focus of ongoing work.

[70] **Acknowledgments.** This research was supported by NSF grant EAR-0838476. E. Matthews provided invaluable assistance at the ANU SHRIMP facility, and G. Kamenov is thanked for assistance with ICPMS analyses at UF. We also thank J. Meert for discussions of the AMS method and use of his analytical facilities. The work benefited from conversations with P. Link and R. McFadden, who also provided sample 05PCRM01 during the early part of the investigation. We are grateful to E. Grudem and A. Carmenate for assistance in the field. The paper has benefited greatly from formal reviews by J. Baldwin and T. Pavlis, as well as from comments by the associate editors.

References

Andronicos, C. L., D. H. Chardon, and L. S. Hollister (2003), Strain partitioning in an obliquely convergent orogen, plutonism, and synorogenic collapse: Coast Mountains batholith, British Columbia, Canada, *Tectonics*, *22*(2), 1012, doi:10.1029/2001TC001312.

Archibald, D. A., T. E. Krogh, R. L. Armstrong, and E. Farrar (1984), Geochronology and tectonic implications of magmatism and metamorphism, southern Kootenay Arc and neighboring regions, southeastern British Columbia. Part II: Mid-Cretaceous to Eocene, *Can. J. Earth Sci.*, *21*, 567–583, doi:10.1139/e84-062.

Baldwin, J. A., A. Graham, and J. W. Desormeau (2011), U-Pb zircon geochronology of meta-anorthosites in the Bitterroot Range, western Montana: Implications for metamorphism and anatexis during core complex formation, *Geol. Soc. Am. Abstr. Programs*, *43*(4), 76.

Beaumont, C., M. H. Nguyen, R. A. Jamieson, and S. Ellis (2006), Crustal flow modes in large hot orogens, in *Channel Flow, Ductile Extrusion and Exhumation in Continental Collision Zones*, edited by R. D. Law et al., *Geol. Soc. Spec. Publ.*, *268*, 91–145.

Bendick, R., and J. Baldwin (2009), Dynamic models for metamorphic core complex formation and unchannelized collapse of thickened continental crust, *Tectonophysics*, *477*(1–2), 93–101, doi:10.1016/j.tecto.2009.03.017.

Bennett, E. H. (1986), Relationship of the trans-Challis fault system in central Idaho to Eocene and Basin and Range extension, *Geology*, *14*, 481–484, doi:10.1130/0091-7613(1986)14<481:ROTTFS>2.0.CO;2.

Breitsprecher, K., D. J. Thorkelson, W. G. Groome, and J. Dostal (2003), Geochemical confirmation of the Kula-Farallon slab window beneath the Pacific Northwest in Eocene time, *Geology*, *31*, 351–354, doi:10.1130/0091-7613(2003)031<0351:GCOTKF>2.0.CO;2.

Brown, R. L., and J. M. Journeay (1987), Tectonic denudation of the Shuswap metamorphic terrane of southeastern British Columbia, *Geology*, *15*, 142–146, doi:10.1130/0091-7613(1987)15<142:TDOTSM>2.0.CO;2.

Brown, S., G. D. M. Andrews, and H. D. Gibson (2010), The Okanagan Valley fault and Okanagan gneiss: New high-precision age constraints on regional extension, metamorphism, and exhumation, *Geol. Soc. Am. Abstr. Programs*, *42*(5), 265.

Cameron, A. (2010), Geochronology of the lower Wildhorse gneiss complex, Pioneer Mtns., Custer County, Idaho, BS thesis, Dep. of Geosci., Idaho State Univ., Pocatello, Idaho.

Carmenate, A., J. J. Vogl, and K. Min (2011), (U-Th)/He evidence for Miocene Yellowstone hot-spot-related uplift in south-central, Idaho, *Geol. Soc. Am. Abstr. Programs*, *43*(5), 276.

Carmichael, D. (1978), Metamorphic bathozones and bathograds: A measure of the depth of post-metamorphic uplift and erosion on the regional scale, *Am. J. Sci.*, *278*, 769–797, doi:10.2475/ajs.278.6.769.

Carr, S. D. (1992), Tectonic setting and U-Pb geochronology of the Early Tertiary Ladybird leucogranite suite, Thor-Odin–Pinnacles area, southern Omenica belt, British Columbia, *Tectonics*, *11*, 258–278, doi:10.1029/91TC01644.

Carr, S. D., and P. S. Simony (2006), Ductile thrusting versus channel flow in the southeastern Canadian Cordillera: Evolution of a coherent crystalline thrust sheet, in *Channel Flow, Ductile Extrusion and Exhumation in Continental Collision Zones*, edited by R. D. Law et al., *Geol. Soc. Spec. Publ.*, *268*, 561–587.

Colgan, J. P., K. A. Howard, R. J. Fleck, and J. L. Wooden (2010), Rapid Middle Miocene extension and unroofing of the southern Ruby Mountains, Nevada, *Tectonics*, *29*, TC6022, doi:10.1029/2009TC002655.

Constenius, K. N. (1996), Late Paleogene extensional collapse of the Cordilleran foreland fold and thrust belt, *Geol. Soc. Am. Bull.*, *108*, 20–39, doi:10.1130/0016-7606(1996)108<0020:LPECOT>2.3.CO;2.

Crittenden, M. D., P. J. Coney, and G. H. Davis (Eds.) (1980), *Cordilleran Metamorphic Core Complexes*, *Mem. Geol. Soc. Am.*, *153*, 490 pp.

Crowley, J. L. (1999), U-Pb geologic constraints on Paleoproterozoic tectonism in the Monashee complex, Canadian Cordillera: Elucidating an overprinted geologic history, *Geol. Soc. Am. Bull.*, *111*, 560–577, doi:10.1130/0016-7606(1999)111<0560:UPGCOP>2.3.CO;2.

Crowley, J. L., R. L. Brown, and R. R. Parrish (2001), Diachronous deformation and a strain gradient beneath the Selkirk allochthon, northern Monashee complex, southeastern Canadian Cordillera, *J. Struct. Geol.*, *23*, 1103–1121, doi:10.1016/S0191-8141(00)00179-6.

Dickinson, W. R. (2002), The Basin and Range Province as a composite extensional domain, *Int. Geol. Rev.*, *44*, 1–38, doi:10.2747/0020-6814.44.1.1.

Diedesch, T. X. (2011), Kinematic analysis of the Wildhorse detachment fault system, Pioneer Mountains, south-central Idaho, MS thesis, Dep. of Geosci., Idaho State Univ., Pocatello, Idaho.

Doughty, P. T., and K. R. Chamberlain (2004), New U-Pb SHRIMP evidence for multiple metamorphic events in the northern U.S. Cordillera: Eocene, Cretaceous, and Late Precambrian (Grenville) events, *Geol. Soc. Am. Abstr. Programs*, *36*(5), 271.

Doughty, P. T., and R. A. Price (1999), Tectonic evolution of the Priest River complex, northern Idaho and Washington: A reappraisal of the Newport fault with new insights into core complex formation, *Tectonics*, *18*, 375–393, doi:10.1029/1998TC900029.

Dover, J. H. (1981), Geology of the Boulder-Pioneer Wilderness study area, Blaine and Custer Counties, Idaho, in Boulder-Pioneer Study area, Idaho, *U.S. Geol. Surv. Bull.*, *1497*, 15–75.

Dover, J. H. (1983), Geologic map and sections of the central Pioneer Mountains, Blaine and Custer Counties, Central Idaho, *U.S. Geol. Surv. Misc. Invest. Ser. Map*, *I-1319*.

Dubiel, R. F., C. J. Potter, S. C. Good, and L. W. Snee (1996), Reconstructing an Eocene extensional basin: The White Sage Formation, eastern Great Basin, in *Reconstructing the History of Basin and Range Extension Using Sedimentology and Stratigraphy*, edited by K. K. Beratan, *Spec. Pap. Geol. Soc. Am.*, *303*, 1–14.

Durk, K. M. (2007), Geochronology of part of the Wildhorse Gneiss Complex, Pioneer Mountains, Custer County, Idaho, BS thesis, Dep. of Geosci., Idaho State Univ., Pocatello, Idaho.

Engebretson, D. C., A. Cox, and R. G. Gordon (1985), Relative motions between oceanic and continental plates in the Pacific Basin, *Spec. Pap. Geol. Soc. Am.*, *206*, 59 pp.

Ewing, T. E. (1980), Paleogene tectonic evolution of the Pacific Northwest, *J. Geol.*, *88*, 619–638, doi:10.1086/628551.

Foster, D. A., and C. M. Fanning (1997), Geochronology of the northern Idaho batholith and the Bitterroot metamorphic core complex: Magmatism preceding and contemporaneous with extension, *Geol. Soc. Am. Bull.*, *109*, 379–394.

Foster, D. A., C. Schafer, C. M. Fanning, and D. W. Hyndman (2001), Relationship between crustal partial melting, plutonism, orogeny, and exhumation: Idaho-Bitterroot batholith, *Tectonophysics*, *342*, 313–350, doi:10.1016/S0040-1951(01)00169-X.

Foster, D. A., P. T. Doughty, T. J. Kalakay, C. M. Fanning, S. Coyner, W. C. Grice Jr., and J. J. Vogl (2007), Kinematics and timing of exhumation of Eocene metamorphic core complexes along the Lewis and Clark fault zone, northern Rocky Mountains, USA, in *Exhumation along Major Continental Strike-Slip Systems*, edited by A. Till et al., *Spec. Pap. Geol. Soc. Am.*, *434*, 205–229.

Foster, D. A., W. C. Grice Jr., and T. J. Kalakay (2010), Extension of the Anaconda metamorphic core complex: $^{40}Ar/^{39}Ar$ thermochronology and implications for Eocene tectonics of the northern Rocky Mountains and the Boulder batholith, *Lithosphere*, *2*, 232–246, doi:10.1130/L94.1.

Foster, G., R. R. Parrish, M. S. A. Horstwood, S. Chenery, J. Pyle, and H. D. Gibson (2004), The generation of prograde P-T-t points and paths; a textural, compositional, and chronological study of metamorphic monazite, *Earth Planet. Sci. Lett.*, *228*, 125–142, doi:10.1016/j.epsl.2004.09.024.

Gans, P. B., M. Wong, and A. T. Calvert (2011), Late Mesozoic and Cenozoic evolution of east-central Nevada: Hinterland tectonics and the origin of metamorphic core complexes, *Geol. Soc. Am. Abstr. Programs*, *43*, 3.

Gao, H., E. D. Humphreys, H. Yao, and R. D. van der Hilst (2011), Crust and lithosphere structure of the northwestern U.S. with ambient noise tomography: Terrane accretion and Cascade arc development, *Earth Planet. Sci. Lett.*, *304*, 202–211, doi:10.1016/j.epsl.2011.01.033.

Gervais, F., and R. L. Brown (2011), Testing modes of exhumation in collisional orogens: Synconvergent channel flow in the southeastern Canadian Cordillera, *Lithosphere*, *3*, 55–75, doi:10.1130/L98.1.

Gervais, F., R. L. Brown, and J. L. Crowley (2010), Tectonic implications for a Cordilleran orogenic base in the Frenchman Cap dome, southeastern Canadian Cordillera, *J. Struct. Geol.*, *32*, 941–959, doi:10.1016/j.jsg.2010.05.006.

Glombick, P., R. I. Thompson, P. Erdmer, and K. L. Daughtry (2006), A reappraisal of the tectonic significance of early Tertiary low-angle shear zones exposed in the Vernon map area (82 L), Shuswap metamorphic complex, southeastern Canadian Cordillera, *Can. J. Earth Sci.*, *43*, 245–268, doi:10.1139/e05-101.

Gordon, S. M., D. L. Whitney, C. Teyssier, M. Grove, and W. J. Dunlap (2008), Timescales of migmatization, melt crystallization, and cooling in a Cordilleran gneiss dome: Valhalla complex, southeastern British Columbia, *Tectonics*, *27*, TC4010, doi:10.1029/2007TC002103.

Haeussler, P. J., D. W. Bradley, R. E. Wells, and M. L. Miller (2003), Life and death of the Resurrection plate; evidence for its existence and subduction in the northeastern Pacific in Paleocene-Eocene time, *Geol. Soc. Am. Bull.*, *115*, 867–880.

Hansen, V. L., and J. W. Goodge (1988), Metamorphism, structural petrology, and regional evolution of the Okanogan complex, northeastern Washington, in *Metamorphism and Crustal Evolution of the Western United States*, *Rubey Colloq. Ser.*, vol. 7, edited by W. G. Ernst, pp. 233–270, Prentice-Hall, Englewood Cliffs, N. J.

Harms, T. A., and R. A. Price (1992), The Newport fault: Eocene listric normal faulting, mylonitization, and crustal extension in northeast Washington and northwest Idaho, *Geol. Soc. Am. Bull.*, *104*, 745–761, doi:10.1130/0016-7606(1992)104<0745:TNFELN>2.3.CO;2.

Henry, C. D. (2008), Ash-flow tuffs and paleovalleys in northeastern Nevada: Implications for Eocene paleogeography and extension in the Sevier hinterland, northern Great Basin, *Geosphere*, *4*(1), 1–35, doi:10.1130/GES00122.1.

Hinchey, A. M., S. D. Carr, P. D. McNeill, and N. Rayner (2006), Paleocene-Eocene high-grade metamorphism, anatexis, and deformation in the Thor-Odin dome, Monashee complex, southeastern British Columbia, *Can. J. Earth Sci.*, *43*, 1341–1365, doi:10.1139/e06-028.

House, M. A., K. V. Hodges, and S. A. Bowring (1997), Petrological and geochronological constraints on regional metamorphism along the northern border of the Bitterroot batholith, *J. Metamorph. Geol.*, *15*, 753–764, doi:10.1111/j.1525-1314.1997.00052.x.

Huerta, A. D., and D. W. Rodgers (1996), Kinematic and dynamic analysis of a low-angle strike-slip fault: The Lake Creek Fault of south-central Idaho, *J. Struct. Geol.*, *18*, 585–593, doi:10.1016/S0191-8141(96)80026-5.

Humphreys, E. D. (2008), Cenozoic slab windows beneath the western United States, in *Ores and Orogenesis: Circum-Pacific Tectonics, Geologic Evolution, and Ore Deposits*, edited by J. E. Spencer and S. R. Titley, *Ariz. Geol. Soc. Dig.*, *22*, 389–396.

Humphreys, E. (2009), Relation of flat subduction to magmatism and deformation in the western United States, in *Backbone of the Americas: Shallow Subduction, Plateau Uplift, and Ridge and Terrane Collision*, edited by S. M. Kay et al., *Mem. Geol. Soc. Am.*, *204*, 85–98.

Janecke, S. U. (1992), Kinematics and timing of three superposed extensional systems, east central Idaho: Evidence for an Eocene tectonic transition, *Tectonics*, *11*, 1121–1138, doi:10.1029/92TC00334.

Janecke, S. U., B. F. Hammond, L. W. Snee, and J. W. Geissman (1997), Rapid extension in an Eocene volcanic arc: Structure and paleogeography of an intra-arc half graben in central Idaho, *Geol. Soc. Am. Bull.*, *109*, 253–267, doi:10.1130/0016-7606(1997)109<0253:REIAEV>2.3.CO;2.

Johnson, B. J., and R. L. Brown (1996), Crustal structure and early Tertiary extensional tectonics of the Omenica belt at 51°N latitude, southern Canadian Cordillera, *Can. J. Earth Sci.*, *33*, 1596–1611, doi:10.1139/e96-121.

Johnston, D. H., P. F. Williams, R. L. Brown, J. L. Crowley, and S. D. Carr (2000), Northeastward extrusion and extensional exhumation of crystalline rocks of the Monashee complex, southeastern Canadian Cordillera, *J. Struct. Geol.*, *22*, 603–625, doi:10.1016/S0191-8141(99)00185-6.

Kent, K. A., J. J. Vogl, and J. M. Meert (2010), Anisotropy of magnetic susceptibility (AMS) and paleomagnetic analysis of a mid-crustal plutonic suite: a record of extension and doming in the footwall of the Pioneer core complex, *Geol. Soc. Am. Abstr. Programs*, *42*(5), 269.

Kruckenberg, S. C., and D. L. Whitney (2011), Metamorphic evolution of sapphirine- and orthoamphibole-cordierite-bearing gneiss, Okanogan dome, Washington, USA, *J. Metamorph. Geol.*, *29*(4), 425–449, doi:10.1111/j.1525-1314.2010.00926.x.

Kruckenberg, S. C., D. L. Whitney, C. Teyssier, C. M. Fanning, and J. W. Dunlap (2008), Paleocene-Eocene migmatite crystallization, extension, and exhumation in the hinterland of the northern Cordillera: Okanogan dome,Washington, USA, *Geol. Soc. Am. Bull.*, *120*, 912–929, doi:10.1130/B26153.1.

Kuiper, Y. D., P. F. Williams, and S. Kruse (2006), Possibility of Channel flow in the southern Canadian Cordillera: A new approach to explain existing data, in *Channel Flow, Ductile Extrusion and Exhumation in Continental Collision Zones*, edited by R. D. Law et al., *Geol. Soc. Spec. Publ.*, *268*, 589–611.

Laberge, J. D., and D. R. M. Pattison (2007), Geology of the western margin of the Grand Forks complex, southern British Columbia: High-grade Cretaceous metamorphism followed by Early Tertiary extension on the Granby fault, *Can. J. Earth Sci.*, *44*, 199–228, doi:10.1139/e06-101.

Link, P. K., K. M. Durk, and C. M. Fanning (2007), SHRIMP U-Pb ages from Archean orthogneiss, Mesoproterozoic paragneiss and Eocene Boulder Creek Pluton, Pioneer Mountains, southcentral Idaho, part of the 2600 Ma Grouse Creek block, *Geol. Soc. Am. Abstr. Programs*, *39*(6), 613.

Link, P. K., A. Cameron, K. M. D. Autenrieth, and C. M. Fanning (2010), Tectonostratigraphy of the Wildhorse gneiss complex, Pioneer Mountains: Neoarchean orthogneiss and overlying Mesoproterozoic Lemhi Group overlie Albion Range Proterozoic quartzite, *Geol. Soc. Am. Abstr. Programs*, *42*(5), 415.

MacCready, T., A. W. Snoke, J. E. Wright, and K. A. Howard (1997), Mid-crustal flow during Tertiary extension in the Ruby Mountains core complex, Nevada, *Geol. Soc. Am. Bull.*, *109*, 1576–1594, doi:10.1130/0016-7606(1997)109<1576:MCFDTE>2.3.CO;2.

Madsen, J. K., D. J. Thorkelson, R. M. Friedman, and D. D. Marshall (2006), Cenozoic to Recent plate configurations in the Pacific Basin: Ridge-subduction and slab window magmatism in western North America, *Geosphere*, *2*, 11–34, doi:10.1130/GES00020.1.

McGrew, A. J., and L. W. Snee (1994), A $^{40}Ar/^{39}Ar$ thermochronologic constraints on the tectonothermal evolution of the Northern East Humboldt Range metamorphic core complex, Nevada, *Tectonophysics*, *238*, 425–450, doi:10.1016/0040-1951(94)90067-1.

Miller, E. L., T. A. Dumitru, R. W. Brown, and P. B. Gans (1999), Rapid Miocene slip on the Snake Range-Deep Creek Range fault system, east-central Nevada, *Geol. Soc. Am. Bull.*, *109*, 1576–1594.

Mueller, K. J., P. K. Cerveny, M. E. Perkins, and L. W. Snee (1999), Chronology of polyphase extension in the Windermere Hills, northeast Nevada, *Geol. Soc. Am. Bull.*, *111*, 11–27, doi:10.1130/0016-7606(1999)111<0011:COPEIT>2.3.CO;2.

Norlander, B. H., D. L. Whitney, C. Teyssier, and O. Vanderhaeghe (2002), Partial melting and decompression of the Thor-Odin dome, Shuswap metamorphic core complex, Canadian Cordillera, *Lithos*, *61*, 103–125, doi:10.1016/S0024-4937(02)00075-0.

O'Neill, R. L., and T. L. Pavlis (1988), Superposition of Cenozoic extension on Mesozoic compressional structures in the Pioneer Mountains metamorphic core complex, central Idaho, *Geol. Soc. Am. Bull.*, *100*, 1833–1845, doi:10.1130/0016-7606(1988)100<1833:SOCEOM>2.3.CO;2.

Parrish, R. R. (1995), Thermal evolution of the southeastern Canadian Cordillera, *Can. J. Earth Sci.*, *32*, 1618–1642, doi:10.1139/e95-130.

Parrish, R. R., S. D. Carr, and D. L. Parkinson (1988), Eocene extensional tectonics and geochronology of the southern Omenica belt, British Columbia and Washington, *Tectonics*, *7*, 181–212, doi:10.1029/TC007i002p00181.

Paterson, S. R., R. B. Miller, H. Alsleben, D. L. Whitney, P. M. Valley, and H. Hurlow (2004), Driving mechansims for >40 km of exhumation during contraction and extension in a continetal arc, Cascades core, Washington, *Tectonics*, *23*, TC3005, doi:10.1029/2002TC001440.

Pattison, D. R. M. (1992), Stability of andalusite and sillimanite and the Al_2SiO_5 triple point: Constraints from the Ballachulish aureole, Scotland, *J. Geol.*, *100*, 423–446, doi:10.1086/629596.

Pattison, D. R. M., and R. J. Tracy (1991), Phase equilibria and thermobarometry of metapelites, in *Contact Metamorphism*, *Rev. Mineral.*, vol. 26, edited by D. M. Kerrick, pp. 105–206, Mineral. Soc. of Am., Chantilly, Va.

Pavlis, T. L., and R. L. O'Neill (1987), Comment on " Extensional deformation with northwest vergence, Pioneer core complex, central Idaho", *Geology*, *15*, 283–284, doi:10.1130/0091-7613(1987)15<283b:CAROED>2.0.CO;2.

Potter, C. J., R. F. Dubiel, S. C. Good, and L. W. Snee (1995), Eocene extension of early Eocene lacustrine strata in a complexly deformed Sevier-Laramide hinterland, northwest Utah and northeast Nevada, *Geology*, *23*, 181–184, doi:10.1130/0091-7613(1995)023<0181:EEOEEL>2.3.CO;2.

Price, R. A., and D. M. Carmichael (1986), Geometric test for Late Cretaceous-Paleogene intracontinental transform faulting in the Canadian Cordillera, *Geology*, *14*, 468–471, doi:10.1130/0091-7613(1986)14<468:GTFLCI>2.0.CO;2.

Rodgers, D. W., P. K. Link, and A. D. Huerta (1995), Structural framework of mineral deposits hosted by Paleozoic rocks in the northeastern part of the Hailey 1° × 2° quadrangle, south-central Idaho, *U.S. Geol. Surv. Bull.*, *2064-B*, 1–18.

Saltzer, S. D., and K. V. Hodges (1988), The Middle Mountain shear zone, southern Idaho; kinematic analysis of an early Tertiary high-temperature detachment, *Geol. Soc. Am. Bull.*, *100*(1), 96–103, doi:10.1130/0016-7606(1988)100<0096:TMMSZS>2.3.CO;2.

Sanford, R. F. (2005), Geology and stratigraphy of the Challis volcanic group and related rocks, Little Wood River area, south-central Idaho, *U.S. Geol. Surv. Bull.*, *2064–II*, 22 pp.

Schmandt, B., and E. Humphreys (2011), Seismically imaged relict slab from the 55 Ma Siletzia accretion to the northwest United States, *Geology*, *39*, 175–178, doi:10.1130/G31558.1.

Silverberg, D. S. (1990) The tectonic evolution of the Pioneer metamorphic core complex, south-central Idaho, PhD thesis, Dep. of Earth, Atmos., and Planet. Sci., Mass. Inst. of Technol., Cambridge.

Skipp, B., L. G. Snider, S. U. Janecke, and M. A. Kuntz (2009), Geologic map of the Arco 30 × 60 minute quadrangle, Idaho, *Map GM-47*, Idaho Geol. Surv., Moscow.

Snider, L. G. (1995), Stratigraphic framework, geochemistry, geochronology, and eruptive styles of Eocene volcanic rocks in the White Knob Mountains area, southeastern Challis volcanic field, central Idaho, MS thesis, Dep. of Geosci., Idaho State Univ., Pocatello.

Spear, F. S., and R. R. Parrish (1996), Petrology and cooling rates of the Valhalla Complex, British Columbia, Canada, *J. Petrol.*, *37*, 733–765, doi:10.1093/petrology/37.4.733.

Sterne, E. J., and K. N. Constenius (1997), Space-time relationships between magmatism and tectonism in the western United States between 120 Ma and 10 Ma: A regional context for the Front Range of Colorado, in *Geologic History of the Colorado Front Range: 1997 RMS-AAPG Field Trip #7*, edited by D. W. Bolyard and S. A. Sonnenberg, pp. 85–100, Rocky Mt. Assoc. of Geol., Denver, Colo.

Tempelman-Kluit, D., and D. Parkinson (1986), Extension across the Eocene Okanagan crustal shear in southern British Columbia, *Geology*, *14*, 318–321, doi:10.1130/0091-7613(1986)14<318:EATEOC>2.0.CO;2.

Teyssier, C., E. C. Ferre, D. L. Whitney, B. Norlander, O. Vanderhaeghe, and D. Parkinson (2005), Flow of partially molten crust and origin of detachments during collapse of the Cordilleran Orogen, in *High-Strain Zones Structure and Physical Properties*, edited by D. Bruhn and L. Burlini, *Geol. Soc. Spec. Publ.*, *245*, 39–64.

Thorkelson, D. J., and R. P. Taylor (1989), Cordilleran slab windows, *Geology*, *17*, 833–836, doi:10.1130/0091-7613(1989)017<0833:CSW>2.3.CO;2.

Thorman, C. H., and L. W. Snee (1988), Thermochronology of metamorphic rocks in the Wood Hills and Pequop Mtns, northeastern Nevada, *Geol. Soc. Am. Abstr. Programs*, *20*, 18.

Umhoefer, P. J., and P. Schiarizza (1996), Latest Cretaceous to early Tertiary dextral strike-slip faulting on the southeastern Yalakom fault system, southeastern Coast Belt, British Columbia, *Geol. Soc. Am. Bull.*, *108*, 768–785, doi:10.1130/0016-7606(1996)108<0768:LCTETD>2.3.CO;2.

Vanderhaeghe, O., C. Teyssier, and R. Wysoczanski (1999), Structural and geochronologic constraints on the role of partial melting during the formation of the Shuswap metamorphic core complex at the latitude of the Thor–Odin dome, British Columbia, *Can. J. Earth Sci.*, *36*, 917–943, doi:10.1139/e99-023.

Vogl, J. J., A. Carmenate, K. Min, D. W. Rodgers, and C. M. Fanning (2010), Extensional and cooling history of the Pioneer core complex, south-central Idaho: Long-lived, episodic extension and implications for regional patterns of extension, *Geol. Soc. Am. Abstr. Programs*, *42*(5), 595.

Vogl, J. J., T. Diedesch, D. Rodgers, and A. Lexvold (2011), A strain gradient within the footwall of the Pioneer core complex, Idaho: complex overprinting of Cretaceous structures by Eocene extensional strain and possible syn-extensional shortening, *Geol. Soc. Am. Abstr. Programs*, *43*(5), 645.

Wells, M. J., L. W. Snee, and A. E. Blythe (2000), Dating of major normal fault systems using thermochronology: An example from the Raft River detachment, Basin and Range, western United States, *J. Geophys. Res.*, *105*, 16303–16327, doi:10.1029/2000JB900094.

Worl, R. G., and K. M. Johnson (1995), Map showing geologic terranes of the Hailey 1 degree × 2 degrees quadrangle and the western part of the Idaho Falls 1° × 2° quadrangle, south-central Idaho, *U.S. Geol. Surv. Bull.*, *2064-A*.

Wust, S. L. (1986), Extensional deformation with northwest vergence, Pioneer core complex, central Idaho, *Geology*, *14*, 712–714, doi:10.1130/0091-7613(1986)14<712:EDWNVP>2.0.CO;2.

T. Diedesch, Department of Earth and Planetary Sciences, University of Tennessee, Knoxville, TN 37996, USA. (tdiedesc@utk.edu)

C. M. Fanning, Research School of Earth Sciences, Australian National University, Canberra, ACT 0200, Australia. (mark.fanning@anu.edu.au)

D. A. Foster, K. A. Kent, and J. J. Vogl, Department of Geological Sciences, University of Florida, Gainesville, FL 32611, USA. (dafoster@ufl.edu; akent927@ufl.edu; jvogl@ufl.edu)

D. W. Rodgers, Department of Geosciences, Idaho State University, Pocatello, ID 83209, USA. (rodgdavi@isu.edu)